Characterization of Polymer Resins and Magnetic Particles for Biofuel Recovery via Solid Phase Extraction

by

Yuchen Wang

A Thesis Presented in Partial Fulfillment
of the Requirements for the Degree
Master of Science

Approved July 2012 by the
Graduate Supervisory Committee:

David Nielsen, Chair
Jean Andino
Cesar Torres

ARIZONA STATE UNIVERSITY

August 2012

ABSTRACT

Due to depletion of oil resources, increasing fuel prices and environmental issues associated with burning of fossil fuels, extensive research has been performed in biofuel production and dramatic progress has been made. But still problems exist in economically production of biofuels. One major problem is recovery of biofuels from fermentation broth with the relatively low product titer achieved. A lot of in situ product recovery techniques including liquid-liquid extraction, membrane extraction, pervaporation, gas stripping and adsorption have been developed and adsorption is shown to be the most promising one compared to other methods. Yet adsorption is not perfect due to defect in adsorbents and operation method used. So laurate adsorption using polymer resins was first investigated by doing adsorption isotherm, kinetic, breakthrough curve experiment and column adsorption of laurate from culture. The results indicate that polymer resins have good capacity for laurate with the highest capacity of 430 g/kg achieved by IRA-402 and can successfully recover laurate from culture without causing problem to *Synechocystis* sp.. Another research of this paper focused on a novel adsorbent: magnetic particles by doing adsorption equilibrium, kinetic and toxicity experiment. Preliminary results showed excellent performance on both adsorption capacity and kinetics. But further experiment revealed that magnetic particles were toxicity and inhibited growth of all kinds of cell tested severely, toxicity probably comes from Co (III) in magnetic particles. This problem might be solved by either using biocompatible coatings or immobilization of cells, which needs more investigation.

DEDICATION

I would like to give special thanks to my family especially my parents and grandparents. Without your strong support I couldn't have made so far through my master's study. Dad and Mom, thank you for your support for my daily life and study. Grandfather, thank you for your influence on choosing my major and makes me find out Chemical Engineering is my favorite.

ACKNOWLEDGMENTS

I would like to give my most sincere gratitude to my advisor, Dr. David Nielsen, for giving me the best and most patient guidance to my research and thesis through these two years. Without this, I couldn't have made this far. Also, I would like to thank him for giving me the opportunity to work in his lab and work on numerous research projects. I would also like to thank Dr. Jean Andino and Cesar Torres for agreeing to serve on my thesis committee.

I would also like to give my thanks to all my labmates: Shawn, Becky, Wei, Jake, Tom, Kyle, Mason, Michael, Ploy, Luis. Thank you for your help in both my research and class. I feel really happy to work with you guys.

At last I also want to thank Raul, Hyun Woo, Dan, Shuqin and Luke for helping me so much with my research projects.

TABLE OF CONTENTS

CHAPTER Page

CHAPTER Page

LIST OF TABLES

LIST OF FIGURES

Figure Page

Chapter 1

INTRODUCTION

1.1 The Importance and growing need for biofuels

Since the 1970s, renewable fuels and materials have attracted significant interest due to high petroleum prices and an awareness of the depletion of fossil fuel reserves. Total United States production of bioethanol (for use as liquid fuel) reached over 18.6×10^6 m^3 (4.86 billion gallons) in 2006. This level of ethanol production, however, represents only about 3% of the gasoline used in the U.S. (538×10^6 m^3 or 140 billion gallons). Meanwhile, the U.S. is targeting to replace 30% of its gasoline needs with renewable fuels by 2030 (Qureshi, Saha et al. 2008). Novel technologies to facilitate the sustainable and economical production of biofuels from renewable resources are required to help bridge this gap.

1.2 Types of liquid biofuels

The most commonly proposed biofuel alternatives to conventional gasoline are ethanol and *n*-butanol, both of which are natural fermentation products. Ethanol is produced as a natural fermentation product by numerous microbes and can be used in petrol engines as a replacement for or additive to gasoline (Thomas, Hynes et al. 1996). The three best characterized ethanol producers include *Saccharomyces cerevisiae, Zymomonas mobilis, and Escherichia coli*, each of differ in terms of their ethanol production ability. For example, using a mutant strain of yeast (*S. cerevisiae* 63M) Laluce *et al.* (2009) achieved an ethanol concentration of 80.8 ± 2.0 g/L in batch fermentation with 200 g/L sucrose and modified synthetic medium described by Thomas *et al.* (1998) (Laluce, Tognolli et al. 2009). Meanwhile, in batch fermentations using native strain of *Z.*

mobilis, Pinilla *et al.* achieved a maximum ethanol concentration of 83.81 g/L and volumetric productivity of 2.28 (g/(L•h)) using Yeast extract-peptone-dextrose (YPD) media with addition of urea (Pinilla, Torres et al. 2011). Yomano *et al.* (2008) later reengineered *E. coli* to achieve ethanol concentration of 40g/L within 48 hours in batch fermentations with xylose added to mineral salts medium (Yomano, York et al. 2008).

Whereas ethanol is useful as a biofuel, when compared to longer chain alcohols it suffers from several performance limitations, including: low energy density, more volatile and explosive, lower flash point, and higher vapor pressure. For these reasons, much recent interest has been directed to the production of longer chain alcohol biofuels such as *n*-butanol. *n*-butanol is a natural fermentation product of several *Clostridium* sp. who produce it by the so called ABE, or acetone-butanol-ethanol fermentation. *C. beijerinckii* BA101, for example, was reported to be able to produce 33g/L ABE in 72 hours under batch fermentation conditions by using glucose or starch as substrate (Ezeji, Qureshi et al. 2004).

While ethanol and *n*-butanol make suitable gasoline alternatives, the most commonly proposed biofuel alternatives to conventional diesel are biologically-derived lipids and/or free fatty acids. Catalytic post-processing steps can convert either into fatty acid esters or alkanes, both of which are compatible with conventional diesel engines. While lipids are known to accumulate in numerous species of algae (Magnuson, Jackowski et al. 1993), direct microbial production of free fatty acids was only recently achieved through metabolic engineering. Recently, for example, the photosynthetic cyanobacterium *Synechocystis* sp. PCC 6803 was engineered to produce 10- through 18-carbon free fatty acids (FFAs) directly from sunlight and CO_2. Productivities of up to 133 ± 12 mg/L culture per day have been reported at a cell density of 1.5×10^8 cells/ml (0.23g of dry weight/liter) (Liu, Brune et al. 2010). The sole use sun light and CO_2 inputs

to produce fatty acid-derived fuels is a significant advantage over heterotrophic biofuel production which first requires the cultivation of fermentable biomass feedstocks.

1.3 Challenges in biofuel production

One common problem encountered in biofuel production arises due to the innate toxicity of the products, which results in feedback inhibition against the producing microbes, limiting achievable titers and productivity. In general, alcohol toxicity against cells is known to be correlated with $logK_{o/w}$ of the alcohol; $K_{o/w}$ is called the octanol/water partition coefficient and is used to provide a relative measure of the hydrophobicity of different molecules. A larger $logK_{o/w}$ will result in a larger hydrophobicity and greater the toxicity, and thus alcohols that have longer carbon chain length are more toxic. For example, feedback inhibition limits maximal ethanol production to final titers of below about 210 g/L (equivalent to for *Saccharomyces cerevisiae* (Walker 1998) while the highest achievable *n*-butanol titers reported in clostridial fermentations are only around 20g/L (Ezeji, Qureshi et al. 2004). *n*-butanol is known to accumulates in the cell membrane, after which it increasing membrane permeability makes it more and more difficult for the cell to maintain homeostasis. As this behavior is concentration dependent, high butanol concentrations ultimately result in a complete loss of microbial activity. Although microorganisms with higher tolerance to longer chain alcohols are being discovered and engineered (Lin and Blaschek 1983; Matsumoto, Ishikawa et al. 2004), the ability to completely eliminate their inhibiting characteristics is unlikely. Thus, the development of process oriented solutions to overcome product toxicity will be required to ultimately achieve the economical and sustainable production of alcohol biofuels.

While alcohol production by microbes faces toxicity problems, microbial FFA production faces its own unique challenges. One problem is difficulty of recovering and

purifying long-chain FFAs from aqueous culture media. Long-chain FFAs are amphiphilic, possessing both a hydrophobic fatty chain and an anionic carboxylic acid group. Thus, long-chain FFAs behave as anionic surfactants in typical microbial culture environments consisting of minimal salt media and around neutral pH (note that the pKa of lauric acid, for example, is 4.64). Under such conditions, extraction by use of non-aqueous phase solvents is impractical due to the need to first acidify the culture medium to protonate the fatty acid (Lalman and Bagley 2004). Without pH adjustment long-chain FFAs just accumulate at the aqueous-organic interface, supporting the formation of stable emulsions (Bravo, Sanchez et al. 2008). Not only is it difficult and costly to acidify large volumes of buffered culture media, but attempting to do so in the presence of viable cells can be particularly problematic.

1.4 *In situ* product recovery

One approach to solving several of the challenges associated with biofuel production is through *in situ* product recovery. *In situ* product recovery is a method that integrates an appropriate separation strategy within a microbial culture in order to removes the products from the fermentation broth as soon as it is produced to ensure that their concentrations will not reach inhibitory levels. Some of the most commonly studied and used methods in biofuel applications have included gas stripping (Baez, Cho et al. 2011), liquid-liquid extraction (Anvari, Pahlavanzadeh et al. 2009), membrane extraction (Bandini and Gostoli 1992), pervaporation (El-Zanati, Abdel-Hakim et al. 2006), and adsorption (Oudshoorn, van der Wielen et al. 2009; Levario, Dai et al. 2012). These strategies will now be presented and described in greater detail.

1.4.1 Liquid-liquid extraction

In situ recovery by liquid-liquid extraction involves using a water- insoluble organic phase that directly contacts the cell culture to extract the desired product. As the product concentration in the extract phase is higher than the fermentation broth and this helps to reduce downstream separation costs (Shi, Zhang et al. 2005). Thus, good extract should have a very high affinity for target and low water solubility, but organic solvents are always toxic and some might provide carbon source for cell as will be discussed in the following. Liquid-liquid extraction has been used for the recovery of numerous inhibitory bioproducts, including most biofuel molecules. For example, Roffler *et al.* (1987) used oleyl alcohol to extract products from ABE fermentations thereby reducing inhibition by end products and improving butanol productivity by 70% versus the control (Roffler, Blanch et al. 1987). Dhamole *et al.* (2012), meanwhile, studied the effects of biocompatibility and extraction ability of several non-ionic surfactants with regards to the recovery of butanol. They showed that the addition of 6 %(vol.) of non-ionic surfactant L62 to the fermentation broth resulted in butanol production 225% higher than the control. The partition coefficient of butanol in L62-water two phase systems in cloud point extraction ranged from 3 to 4. A considerable enrichment of butanol (6-times) was achieved in the surfactant-rich phase over the control. In addition, the downstream process volume was reduced by 4 to 6 times. But a major problem for *in situ* extraction is the toxicity of commonly used organic solvents. Also from Dhamole *et al.* (2012), 3% L64 reduced the AB yield whereas Triton X 114 (3%) inhibited the AB production (Dhamole, Wang et al. 2012). The biocompatibility of a particular solvent depends on the organism employed, thus requires solvent screening (Martik, Rosenberg et al. 1995). Another problem is bioavailability; some bacteria may use the extract as carbon source for growing, thus making screening for non-bioavailable solvent a necessity.

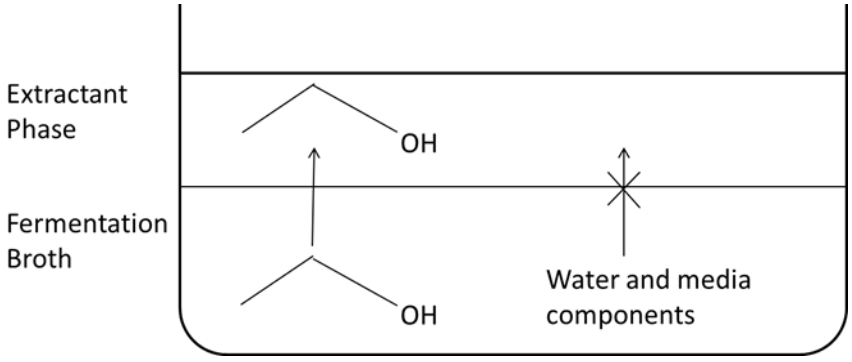

Figure 1.1. Schematic diagram of liquid-liquid extraction in ISPR.

1.4.2 Gas stripping.

Gas stripping is a process in which volatile solutes (lower alcohols, for example) are removed from the fermentation broth and into a 'stripping gas' that is bubbled through the culture. Relative to other *in situ* recovery processes, gas stripping offers several potential advantages. For example, it only removes volatile solvents and not essential nutrients or unwanted byproducts. Also, the stripping gases are clean and do not interact with or inhibit the microorganisms. Solvents stripped can be recovered by condensation or by adsorption. One of the earliest studies conducted was by Liu and Hsu. (1990) in which they applied gas stripping to ethanol fermentation and demonstrated that: (1) the cell concentration increases with increase in the stripping factor (which is determined by volumetric flow rate of stripping gas, gas phase mass transfer coefficient, vapor-liquid equilibrium coefficient, transfer area per unit liquid volume and volume of liquid phase in the reactor) for a given dilution rate, (2) the substrate consumption increases by the stripping factor for a given dilution rate (equal to volumetric flow rate divided by volume of liquid phase), (3) ethanol concentration in the broth decreases with an increase in the stripping factor for a given dilution rate, and (4) ethanol productivity increases with increase in the stripping factor for a given dilution rate (Liu and Hsu 1990).

In a later work, T.C. Ezeji *et al.* (2003) used gas stripping for *in situ* product recovery during ABE fermentation and found that productivities and yield were improved up to 200 and 118%, respectively, as compared to a traditional batch fermentation. In a batch reactor *C. beijerinckii* BA101 utilized 45.4 g glucose/L and produced 17.7 g/L total ABE, while in the integrated process it utilized 161.7 g glucose/L to produce 75.9 g/L total ABE. However, they also encountered several limitations associated with the use of gas stripping, including low selectivity. For example, the selectivity for butanol in their experiment is only approximately between 6.67 and 13.23, another problem was water loss in fermentation broth due to the reason that stripping gas not only take out desired product but also water, to compensate for water loss, oxygen-free distilled water was added at intervals into the reactor to maintain a constant liquid level (Ezeji, Qureshi et al. 2003). That's one of the reasons that make researchers investigating another *in situ* product recovery method: pervaporation.

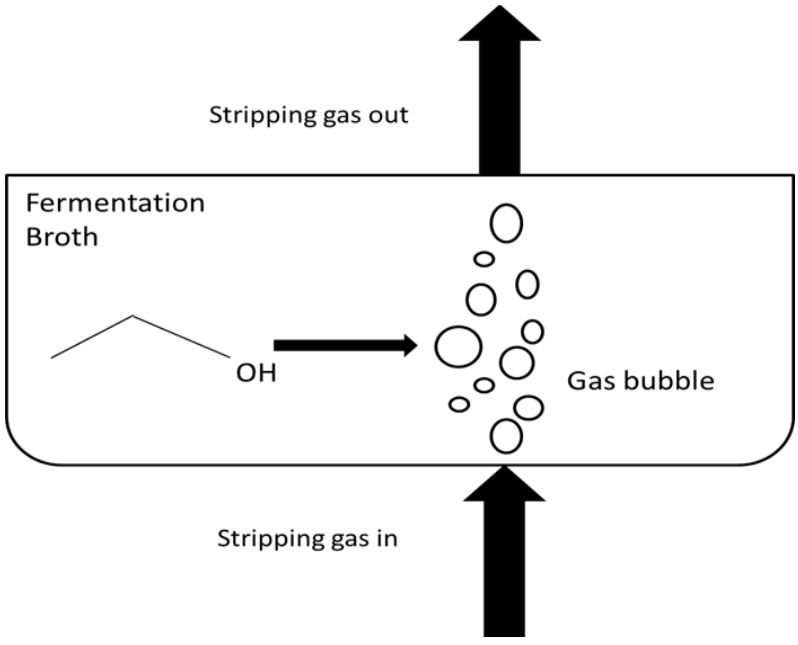

Figure 1.2 Schematic diagram of gas stripping in ISPR.

1.4.3 Pervaporation.

Pervaporation is a process in which a liquid mixture is fed to a membrane and, driven a partial pressure difference across the membrane created by vacuum application on the permeate side, volatile components of the mixture components are selectively transported through the membrane and evaporated on the other side of the membrane. Pervaporation has advantages in separating azeotropes, close-boiling point mixtures and thermally sensitive compounds when compared to distillation; another advantage of pervaporation relative to gas stripping, adsorption, and liquid-liquid extraction is that it doesn't have harmful effect on cells. Qureshi *et al.* (2001) used silicalite–silicone composite membrane for pervaporative recovery of acetone and butanol from fermentation broths. They showed that in the integrated fed-batch reactor the solvent yield (butanol and acetone) was higher (0.34–0.37) than the batch reactor (0.29–0.30). More importantly, it was also found that the silicalite–silicone composite membrane was not fouled by the fermentation broth and selectivities of butanol and acetone were relatively high, ranging from 95-200 for butanol and 40 for acetone (Qureshi, Meagher et al. 2001). Kaewkannetra *et al.* (2011) used a 500 ml bench scale membrane reactor assembled with a pervaporation system, the membranes had a dimension of 3.6 cm in diameter and surface area of 10.2 cm^2 and were added into a membrane unit outside the bioreactor. In their work, the separation of two types of mixtures was studied using cellulose acetate membranes: ethanol–water mixture and fermented sweet sorghum. Different ethanol concentration, operation time and temperature were investigated. They found out that permeate fluxes, selectivity and percent separation declined significantly under all operating conditions in the presence of sweet sorghum fermentation broth when compared to the binary mixture, indicating the problem of fouling of membrane (Kaewkannetra, Chutinate et al. 2011), which was also observed in study by Garc á *et al.*

(2011) in which they proposed membrane used for pervaporation might be fouled by other metabolites or medium components such as sugar or salts (Garcí a, Pä kkilä et al. 2011). In addition to this pervaporation also suffers from problems such as low selectivity at high flux or low flux at high selectivity.

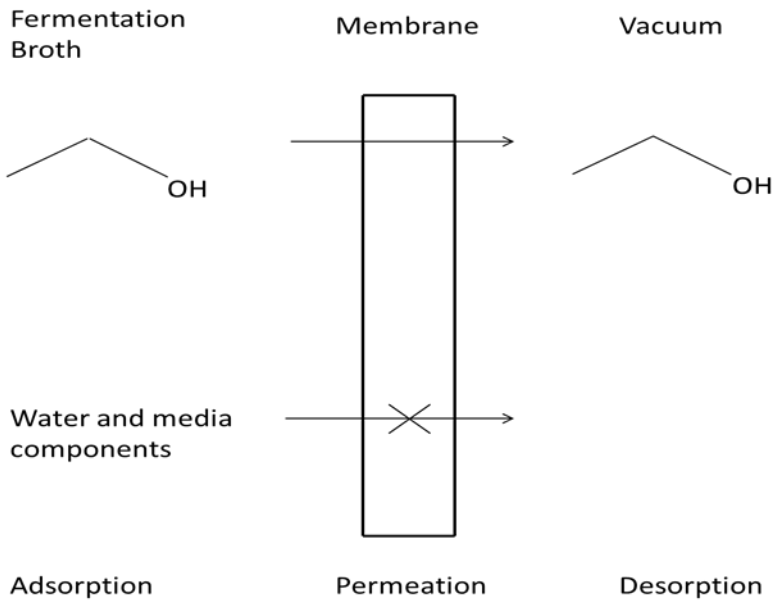

Figure 1.3 Schematic diagram of pervaporation in ISPR.

1.4.4 Membrane extraction

Membrane extraction (also called 'perstraction') is similar to liquid-liquid extraction; however a permeable membrane is also used to provide physical separation between the two liquid phases. Because the solvent phase is not in direct contact with the aqueous phase, phase dispersion, toxicity and bioavailability can be eliminated. Bandml *et al.* (1992) applied a special gas membrane to separate ethanol from fermentation broth. In this case, the membrane is in contact on both sides with aqueous solutions at pressures lower than the pressure needed to displace the gas phase in the pores. As a consequence a gaseous phase is entrapped inside the membrane pores; while at both pore entrances a

gas-liquid interface is located, separating the outer non-wetting liquids from the internal gaseous phase. They found out that the ratio between the final ethanol of the extract and that of the feed (can also be considered as ethanol distribution coefficient) is slightly above 0.8 in isothermal extraction, whereas values at least equal to 0.5 have been considered satisfactory, which means in this case performance of membrane extraction is acceptable. But they also implied when the process is applied to whole fermentation broths instead of synthetic ethanol-water mixtures: 1) membrane fouling may reduce the flux and alter the selectivity, 2) proteinaceous and other organic compounds of the broth may reduce the penetration pressure of the membrane, so that the membrane itself is no longer an effective barrier for the liquid phase (Bandini and Gostoli 1992). There are also other problems associated with membrane extraction. Isono *et al.* (1999) used hydrophobic microfiltration membrane for phase separation of an alcohol/aqueous mixture. Some of the membranes they used, such as NTF-52005 and FV, shrank after experiment (Y. Isono and M. Nakajima 1999).

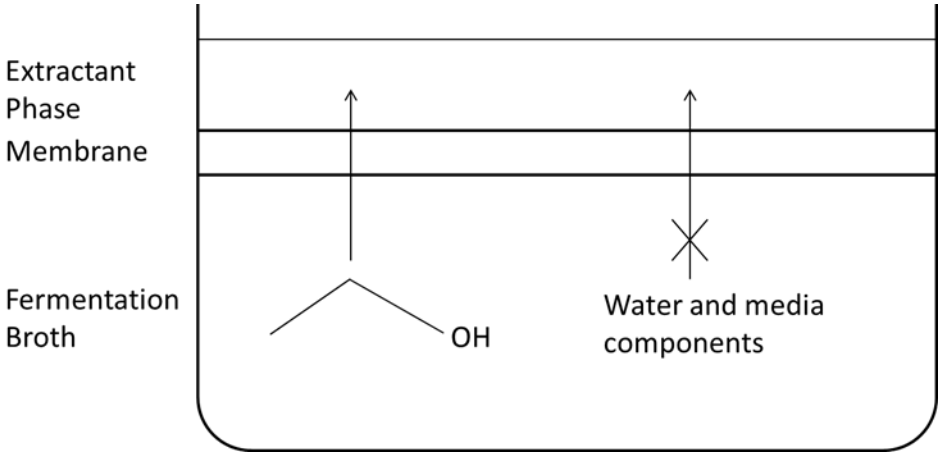

Figure 1.4 Schematic diagram of membrane extraction in ISPR.

1.4.5. Adsorption

Adsorption is a recovery method that uses solid adsorbents, such as polymeric resin, activated carbon and zeolites, for example, to adsorb products from the culture medium. Effective adsorbents are usually porous materials with very large surface areas. Adsorbates can be adsorbed by either hydrophobic interactions (i.e., van Der Waals forces) or by ion exchange. Adsorbed products can later be recovered by heating the hydrophobic adsorbent or by using elution protocol for ion exchange adsorbent. This step also serves to regenerate the adsorbent so that it can be re-used in subsequent cultures. Adsorption allows separation of biofuels from bulk aqueous phase so that downstream processing can be performed only on the relatively small amount of adsorbent, thus making energy efficient recovery possible.

Researchers have studied and characterized various kinds of adsorbents for the recovery of biofuel molecules in recent years, including, but not limited to: 1) polymer resins (Nielsen and Prather 2009; Nielsen, Amarasiriwardena et al. 2010) , 2) zeolites (Adnađević, Mojović et al. 2007; Oudshoorn, van der Wielen et al. 2009; Saravanan, Waijers et al. 2010), and 3) carbonaceous solids (Levario, Dai et al. 2012).

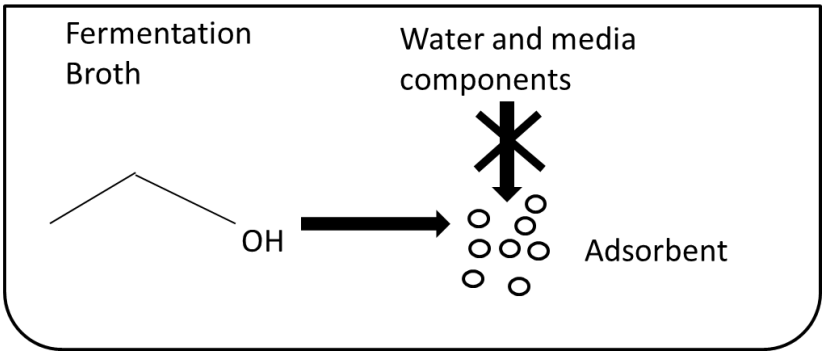

Figure 1.5 Schematic diagram of adsorption in ISPR.

1.4.5.1 Polymer resins. One of the early studies using polymer resins were conducted by Groot *et al.* (1986), who found that with addition of XAD-8 (a kind of polymer resin that

can adsorb *n*-butanol) to fermentation broth, more *n*-butanol was produced than blank fermentation due to removal of the inhibiting product. But they also found with addition of the resins such as XAD-2 and XAD-4, product composition of fermentation mainly consists of acids, possibly due to adsorption of acids or medium components that can lead to a more acidic fermentation course. which means fouling of adsorbents exists (Groot and Luyben 1986). Nielsen *et al.* (2009) screened a variety of resins for their ability to uptake *n*-butanol in aqueous solution with an initial concentration of 20g/L (or 270 mM) (similar to toxicity limit to *C. acetobutylicum*). The resin they studied can be divided into the following groups based on their corresponding monomers: poly(styrene-co-DVB), poly(ester), poly(acrylates), poly(styrene-*co*-butadiene), poly(urethane) and poly(ethylene-*co*-vinyl acetate). They found out that poly(styrene-*co*-DVB) (the one with the highest hydrophobicity) derived resins generally display the greatest affinity for *n*-butanol. For instance, Dowex Optipore L-493 and SD-2 were able to reduce the aqueous *n*-butanol concentration by 85 and 83% while achieving specific loadings of *n*-butanol of 175 and 152 g/kg resin respectively. In the follow up experiment, they used SD-2 to test its ability for *in situ* product recovery. With the addition of 50g/L SD-2 to *C. acetobutylicum* ATCC 824 fermentation broth, effective *n*-butanol titers as high as 2.22% (w/v) was achieved, well above the inhibitory threshold of *C. acetobutylicum* ATCC 824, and nearly twice that of traditional, single-phase fermentations(Nielsen and Prather 2009). In a more recent study, Nielsen *et al.* (2010) studied adsorption capacity of six kinds of resin (all poly(styrene-co-DVB) resins) on eight different alcohols. They successfully found out the correlation between equilibrium partitioning coefficient and alcohol's hydrophobicity. Also they showed resins with a non-polar monomeric structure and high specific surface area provided the highest overall adsorption of each of the studied compounds and longer chain alcohols were subject to greater adsorption due to their

increasingly hydrophobicity. This study provides the first demonstration of the ability of hydrophobic polymer resins to serve as effective *in situ* product recovery (ISPR) devices for the production of second generation biofuels(Nielsen, Amarasiriwardena et al. 2010). However, the adsorbent poly(styrene-co-DVB) has a glass transition temperature of only 95^{o}C, whereas the boiling point of n-butanol is 117^{o}C at normal conditions (1atm). Usually resins are heated to recover biofuel and this might change the structure of the resin, therefore affecting its adsorption capacity, thus developing resin with higher thermostability is required.

1.4.5.2 Zeolites. Zeolites are microporous, aluminosilicate minerals and commonly used commercial adsorbents. Zeolite materials have the advantages of highly-ordered pore structure and high thermal stability. One of the earliest studies was conducted by Maddox (1982) using silicalite to adsorb butanol from fermentation liquors. It was shown that an adsorption capacity of 85mg butanol/g silicalite could be achieved. This provided an alternative to distillation for product recovery and may alleviate product inhibition during fermentation (Maddox 1982). Oudshoorn *et al.* (2009) have proven high silica zeolite CBV28014 to adsorb butanol selectively over water, while it also showed a higher affinity for butanol than for acetone and ethanol, making it a promising candidate for in situ product recovery of *n*-butanol from real culture systems (Oudshoorn, van der Wielen et al. 2009). In a more recent study, Saravanan *et al.* (2009) showed that commercially available zeolites (CBV28014 and CBV901) can quickly and almost completely adsorb *n*-butanol from aqueous solutions containing ~1%wt of *n*-butanol. The adsorption capacity of those zeolites appeared to be around 120 mg *n*-butanol/g zeolite, and remained constant until the equilibrium *n*-butanol concentration was as low as 0.04 wt% (Saravanan, Waijers et al. 2010). Sharma *et al.* (2011) later synthesized MEL type

zeolites and applied them to *n*-butanol adsorption. They found the maximum *n*-butanol adsorption capacity of a MEL6 zeolite to be 222.24 mg/g at 303K with an initial *n*-butanol concentration of 2g/L, much larger than other zeolite materials tested, including high silica zeolite CBV28014 (116.0 mg/g), ZSM-5 (160.58 mg/g), silicalite (97.0 mg/g) and ZSM-5 (110.0 mg/g) (Sharma and Chung 2011). However, it has also been shown that many the zeolites suffer from slow hydrolysis and degradation in aqueous systems, such as those used as fermentation broths (Cook, Cllley et al. 1982). Thus, the chemical instability of zeolites may reduce their long term utility for *in situ* recovery.

1.4.5.3 Activated carbon. In 1986, Groot *et al*. studied adsorption performance of two active carbons (Norit ROW 0.8 and W52) in both *n*-butanol/isopropanol fermentation and model solutions. Norit ROW 0.8 was found capable of adsorbing the highest amount of *n*-butanol and reached a specific loading capacity of ~250 mg/g (or 3400 mmol/kg) at an initial aqueous *n*-butanol concentration of ~15 g/L (or 200 mM). However, fouling problems were also observed in their study. For example, they observed decolorization of medium which indicated co-adsorption of medium components (Groot and Luyben 1986). Later, Silvestre-Albero *et al.* (2009) studied ethanol removal by using a series of activated carbon. The highest adsorption capacity observed was 74g ethanol/kg activated carbon achieved with AC40. What is more interesting , however, is that they also went on to demonstrate that activated carbons can be easily regenerated by air stripping at room temperature (more than 98% desorption/recovery), which is preferable for reducing downstream operation cost (Silvestre-Albero, Silvestre-Albero et al. 2009). Levario *et al.* (2011) recently tested adsorption capacity of four mesoporous carbons on both ethanol and *n*-butanol. They found that *n*-butanol was adsorbed more extensively than ethanol, which is consistent with a hydrophobic adsorption mechanism. They also measured and

compared the kinetics of *n*-butanol adsorption by their carbon powders to commercially available, hydrophobic polymer adsorbents with similar specific surface area. The findings suggested that, due to the regular pore morphology and structure of mesoporous carbons, adsorption rates by these materials were 1–2 orders of magnitude greater than commercial polymer adsorbents. Further studies went on to show that multiple cycles of adsorbent regeneration and re-use could be performed with no impact on either adsorption equilibrium or kinetics. Thus, the high chemical and thermal stability of mesoporous carbons provide advantages over other commonly available biofuel adsorbents, such as polymers and zeolites (Levario, Dai et al. 2012).

1.5 Biofuel recovery using adsorption columns.

Besides adding adsorbents directly to fermentation cultures, researchers have also studied their external use for product recovery by way of adsorption columns through which the culture medium is circulated. This operation brings certain advantages, including the fact it avoids the need to recovery adsorbents from fermentation broths after their use, thus avoiding the cost of solids handling. The most commonly used column adsorption schemes are packed bed and expanded bed adsorption and their scheme are show in Figure 1.6.

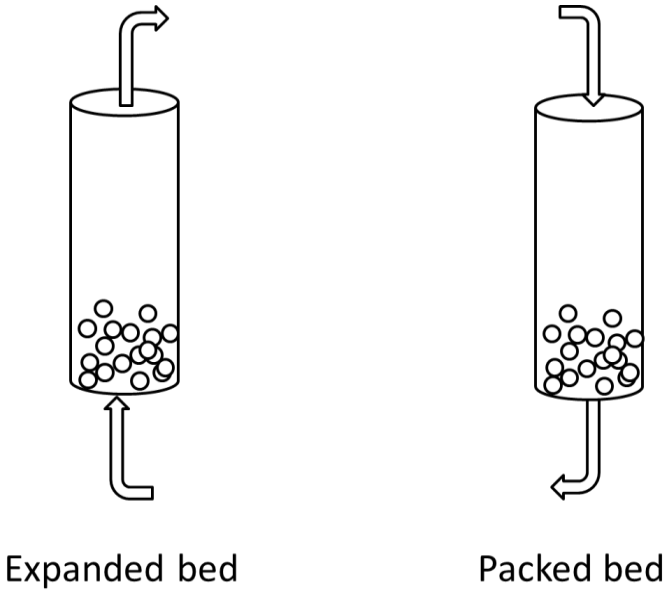

Figure 1.6 Schematic diagram of packed and expanded bed adsorption

Packed bed has the advantages of higher efficiency but pressure will build up, which is stressful to cells. Under certain conditions, the breakthrough time in an expanded-bed adsorber is considerably shorter than that in a comparable fixed-bed adsorber. Nevertheless, several problems, such as excessive head loss, air binding, and fouling with biological and particulate matter are associated with packed-bed operation, but these problems are significantly reduced in fluidized-bed adsorption (Veeraraghavan and Fan 1989). Jones *et al.* (2011) studied the recovery of ethanol by activated carbon using packed bed adsorption. They proved that intermittent ethanol extraction was effective in prolonging and enhancing the production of ethanol in the fermentation broth. Eighty percent more ethanol was produced during the experiment with externally located activated carbon columns. Which is a result of maintaining ethanol fermentation medium concentrations below 20 ~ 30 g/L, smaller than toxicity limit. This study suggests that column adsorption is a potential effective method in recover biofuels (Jones, Gandier et al. 2011).

1.6 Structure of the thesis:

With recent development of microorganisms capable of producing long chain free fatty acid biofuel precursors, effective product recovery strategies need to be developed. Adsorption has the potential to be effectively recover long chain free fatty acids, however, previous research employing polymer resin adsorbents has principally focused on the recovery of alcohol biofuels. Chapter 2 focuses first on characterizing the equilibrium and kinetic adsorption behavior of lauric acid by numerous commercially-available polymer resin adsorbents of different physical properties and ionic functionality. Resin adsorbents were then studied in fixed and expanded bed columns as applied to both lauric acid recovery from model solutions and also from growing cultures of engineered *Synechocystis* PCC 6803.

Whereas polymer resin adsorbents have been previously applied for the recovery of alcohol biofuels, they suffer from several limitations such as low thermal stability. Mesoporous carbon adsorbents have been shown capable of addressing these limitations; however they are difficult to control in culture environments. Chapter 3 focuses on characterizing novel magnetic mesoporous carbon adsorbents for the recovery of alcohol biofuels. As a result of their magnetic functionality, these adsorbents can be readily recovered from aqueous media with minimal energy requirements following biofuel adsorption. Although there has been great advancement in searching for adsorbents for *in situ* recovery of alcohols, such as high selectivity, stability and capacity, there are disadvantages associated with almost each kind of adsorbent. Magnetic mesoporous carbon adsorbents have been investigated and characterized in terms of their equilibrium and kinetic adsorption and biocompatibility. At last, in Chapter 4, some suggestions for future work are presented and discussed.

Chapter 2

FATTY ACID RECOVERY BY ADSORPTION WITH POLYMER RESINS

2.1 Materials and Methods

2.1.1 Adsorbents and Chemicals.

A selection of anion exchange, hydrophobic, and mixed-mode resins (their properties are summarized in Table 2.1) were purchased from Sigma-Aldrich (St. Louis, MO). Sodium laurate was also purchased from Sigma-Aldrich with a purity of 99%-100%.

2.1.2 Analytical Methods.

Laurate concentration in model aqueous solutions (i.e., used in adsorption isotherm experiments, kinetic experiments, and column breakthrough experiments) was determined by total carbon (TC) analysis (TOC-V_{CSH}, Shimadzu Scientific Instruments, USA) equipped with a combustion catalytic oxidation/non-dispersive Infrared (NDIR) gas analyzer and operated according to the High-Temperature Combustion Method, equivalent to 5310B in Standard Methods (Ackers 1982). Laurate concentration in real culture system was analyzed by Prof. Daniel Brune from School of Life Sciences at ASU by using Liquid chromatography–mass spectrometry (LC-MS). Nutrition analysis was performed by using Ion chromatography (IC) analysis. Samples were filtered through a 0.2-mm membrane filter (GD/X, Whatmann, Piscataway, NJ) and analyzed by an ion chromatograph(ICS-3000, Dionex, Sunnyvale, CA) equipped with anion exchange column (IonPac AS18, Dionex). Scanning Electron Microscope (SEM) imaging was performed using the following protocol: 1) resin beads were air-dried in porcelain spot-

plates, 2) resin beads were mounted on aluminum specimen stubs with conductive tape, 3) sputter-coated in a Technics Hummer-II sputter-coater with approximate 15 nm of gold-palladium, 4) imaged in a JEOL JSM6300 SEM operated at 15 kV using 39 mm working distance. Images were acquired with an IXRF model 500 digital processing system.

2.1.3 Determining the equilibrium adsorption behavior of laurate on different commercial adsorbents

A range of commercial adsorbent resins including anion exchange resins, hydrophobic resins, and mixed mode resins were selected for characterization. For comparison, the carbonaceous molecular sieve Carboxen 572 was also studied. Relevant properties of all adsorbents are summarized and compared in Table 2.1.

Table 2.1. Physical properties of adsorbents screened in this study (as reported by their manufacturers).

Type	Resin	Functional Group	Matrix	Capacity (meq/g)[1]	Pore Size (nm) / Specific Surface Area (m^2/g)	Moisture Content (%)	Max Swelling in Water (%)
Anion exchange	Amberlite IRA-958	quaternary ammonium (strong base)	poly-acrylate	4.1	- / -	66-72	-
	Amberlite IRA-67	tertiary amine (weak base)	poly-acrylate (gel)	5.6	- / -	56-64	30
Mixed-mode	Amberlite IRA-900	trimethyl ammonium (strong base)	pS-DVB	4.2	- / -	58-64	25
	Amberlit	trimethyl	pS-	3.8	- / -	49-60	30

	e IRA-402	ammonium (strong base)	DVB (gel)				
	Dowex Optipore SD-2	tertiary amine (weak base)	pS-DVB	0.8	5 / 800	50-62	5
Hydro-phobic	Dowex Optipore L-493	none	pS-DVB	n.a.	4.6 / 1100	50-65	5[2]
	Carboxen 572	none	carbon	n.a.	1.1 / 1100	-	-

n.a.: not applicable; pS-DVB: poly(styrene-*co*-divinylbenzene); -: not provided by manufacturer

[1] by dry weight; [2] assumed from SD-2

Anion exchange and mixed mode resins were first soaked in 1mol/L NaOH and then in 1mol/L HCl each for 6 hours. These resins were then thoroughly rinsed with and stored in deionized water. These steps activated cationic functional groups, leaving the resins in their chloride form. Hydrophobic resins were washed and stored in deionized water. All resins were briefly dried by vacuum filtration for 30 minutes before conducting equilibrium adsorption experiments. Carbon molecular sieve were used directly without any preparation.

For all equilibrium adsorption experiments, 0.2 g adsorbent was added to a 22ml glass vial containing 20ml sodium laurate solution with an initial concentration ranging from 0.5-5 g/L. Glass vials were then shaken at 200 rpm and at 25 ^{o}C for 24 hours to allow equilibrium to be reached. In the end, 10ml of the equilibrated aqueous phase from each vial was sampled for TC analysis to determine laurate concentrations. Specific loading of laurate adsorbed at equilibrium (q_e) was then determined by the following mass balance relationship:

$$q_e = \frac{(C_{aq,0} - C_{aq,e})V_{aq}}{m} \quad (2.1)$$

where $c_{aq,o}$ and $c_{aq,e}$ are the initial and equilibrated laurate concentrations in the aqueous phase, respectively, V_{aq} is the volume of the aqueous phase, and m is the mass of adsorbent.

2.1.3.1 Modeling of adsorption equilibrium. Experimental adsorption equilibrium data ($C_{aq,e}$ and q_e) were fit to both Langmuir and Freundlich models, represented by Equations 2.2 and 2.3, respectively:

$$q_e = \frac{q_{max} C_{aq,e}}{K_d + C_{aq,e}} \tag{2.2}$$

$$q_{eq,\,F} = k_F * C_{aq}^{(1/n)} \tag{2.3}$$

wherein $q_{eq,L}$ and $q_{eq,F}$ are the loading capacities as predicted by the Langmuir and Freundlich equations, respectively, k_L and k_F are the adsorption constants of the Langmuir and Freundlich equations, respectively, $q_{eq,max}$ is the monolayer adsorption or maximum loading capacity, and n is the Freundlich exponent. Model parameter estimates were obtained from experimental data via nonlinear least-squares regression on using the intrinsic MATLAB® function *nlinfit*. Error associated with all parameter estimates were reported at one standard deviation.

2.1.4 Determining the adsorption kinetics of laurate on different commercial adsorbents

To rate of laurate adsorption on different commercial adsorbents, dynamic experiments were conducted for the resins listed in Table 2.1. In these experiments, 0.5 g resin (prepared as mentioned above was added to a 250 ml flask containing 100 ml of a 2 g/L sodium laurate solution. Flasks were then stirred at 25 ^{o}C on a platform shaker at 200 rpm. During the experiment, 0.1 mL aqueous samples were taken at regular time intervals

for a total time of 120 min. Although 20 samples were taken (2 mL removed in total), the total volume change over the course of the experiment was smaller than 2 % and thus ignored. All samples were diluted 100-times by addition of 9.9 ml deionized water to prepare samples for TC analysis to determine laurate concentrations.

2.1.4.1 Modeling of adsorption kinetic. Dynamic adsorption data wre fit to each of pseudo first order, pseudo second order, and pore diffusion models, as shown in Equations 2.4-6, respectively:

$$\frac{dq}{dt} = k_1(q_e - q) \tag{2.4}$$

$$\frac{dq}{dt} = k_2(q_e - q)^2 \tag{2.5}$$

$$\varepsilon_p \frac{\partial C_p}{\partial t} + \frac{\partial q}{\partial t} = \frac{\varepsilon_p D_p}{r^2} \frac{\partial}{\partial r}\left(r^2 \frac{\partial C_p}{\partial r}\right) \tag{2.6}$$

where k_1 and k_2 are the pseudo first and second order mass transfer coefficients, respectively. Using the the pore diffusion model, ε_p is porosity, C_p is laurate concentration in adsorbent pores, r represents radial position in the adsorbent particle, and D_p is diffusivity in the adsorbent pores. In order to solve the pore diffusion model, the following equation that models the laurate concentration in the bulk aqueous phase is also required:

$$\frac{dC_{aq,b}}{dt} = -\frac{3H}{R} \varepsilon_p D_p \frac{dC_p}{dr} \tag{2.7}$$

where $C_{aq,b}$ is the laurate concentration in the bulk aqueous phase, R is the radius of the adsorbent particle, and H is the solid–liquid ratio. Equations 2.6 and 2.7 were solved based on the following initial (IC) and boundary conditions (BC):

IC: @ $t = 0$: $q = 0$, $C_p = 0$, $C_{aq,b} = C_{aq,0}$

BC_1: @ $r = R$: $C_p = C_{aq,b}$

BC_2: $@\ r = 0$: $\frac{\partial C_p}{\partial t} = 0$

where $C_{aq,0}$ is the initial laurate concentration in the aqueous solution. Estimates of diffusion coefficients were obtained via least-squares regression with the objective of minimizing sum of square errors (SSE).

2.1.5 Breakthrough analysis of fixed and expanded bed adsorption

Breakthrough curve experiments were performed to test the performance of adsorbent resin columns, as well as the effects of parameters such as flow rate and bed configuration (namely fixed bed or expanded bed). Breakthrough characterizations experiments were performed using a glass column (Kontes FlexColumn™, 11 mm I.D. x 300 mm length; Kimble Glass Co., Vineland, NJ) containing 4 g adsorbent resin. Columns were fed with an aqueous solution containing 2 g/L sodium laurate at a constant rate (5 or 10 mL/min). Samples of the column's aqueous effluent were collected at regular intervals for a period of up to 200 min for flow rates of 5 mL/min or 100 min for flow rates of 10 mL/min. This corresponded to the processing of a total of 1 L of feed solution in each case. All samples were diluted in deionized water 20 times and analyzed for laurate content by total carbon analysis. The breakthrough time (t_b) was taken as the time at which the sodium laurate concentration in the effluent equaled 5% of the feed (i.e., 0.1 g/L).

2.1.6 Fatty acid adsorption from a culture of engineered cyanobacteria

To test the performance and utility of adsorbent of resins for the recovery of fatty acids from active cultures, a series of experiments were performed in collaboration with Prof. W. Vermaas of the School of Life Sciences at ASU, and with the aid of several

of his students and researchers (S. Li, D. Brune). Their group previously engineered a strain of photosynthetic cyanobacteria *Synechocystis* TE/Δslr1609, to produce and excrete laurate from sunlight and CO_2. Cells were cultured in 2 L flasks containing 1.4 L BG-11 medium with the following concentration: $NaNO_3$: 17.53 mmol/L, $MgSO_4 \cdot 7H_2O$: 304.3 μmol/L, $CaCl_2 \cdot 2 H_2O$: 244.9 μmol/L, Citric acid: 31.24 μmol/L, NaEDTA 2.8 μmol/L, ferric ammonium citrate: 22.64 μmol/L, Na_2CO_3: 188.7 μmol/L and K_2HPO_4 175.1 μmol/L. Cultures were inoculated to an initial OD_{730} of about 0.5 before then being aerated with house air at a rate of 4 L/min, exposed to light at 200 μmol photon/m^2/s, and maintained at 30 ^oC. Growth was routinely monitored twice per day according to OD_{730}. In addition, flasks were measured every day for both nutrition analysis and fatty acid content. To fatty acid analysis sample, 20 μL 0.5mol/L EDTA was added to avoid their precipitation.

To separate laurate from cultures, nearly every 7 days cultures were circulated by pumping at a rate of about 55ml/min through an adsorption column and returned back to the culture flask. While circulating, aqueous samples were taken every 0.5 to 1.5 h for a total period of 5.5 h. The adsorption column used was a 120 mm long by 25 mm inner diameter Flex-Column® (Kimble Chase, NJ, USA) containing 20 g Amberlite IRA-900 resin. IRA-900 was selected due to its relatively high loading capacity and faster adsorption kinetics. Resins were prepared as described above, however, they were also further treated with an excess of sterile BG-11 medium to be equilibrated to the culture environment, thereby avoiding deleterious interaction with anionic media components. Columns were operated in either fixed or expanded bed mode simply be reversing position of the column inlet feed stream, as appropriate. Figure 2.1 shows the column adsorption system.

Figure 2.1 Plot for in situ laurate recovery using column adsorption

2.1.7 Determining interactions of anion echange resins with inorganic media components

To further investigate the reversible adsorption of BG-11 media anions by IRA-900, resins were added to 20 mL BG-11at different solid to liquid ratios (from 0 g resin/L BG-11 to 10 g resin/L BG-11). Samples were shaken on a platform shaker at room temperature and 150 rpm for 24 hours and analyzed by Ion Chromatography (IC) analysis.

2.1.8 Investigating fouling of adsorbents by cells

In addition to studying the impact of laurate recovery by expanded bed adsorption we also investigated potential practical complications associated with this strategy. This included the potential for biofilm formation upon the different resin particles. Biofouling is a potential problem because it reduces adsorption surface area,

increases diffusional resistances, and might also complicate downstream processing for product recovery and adsorbent regeneration. To investigate this prospect, 0.2 g different resins (including IRA-900, IRA-958, MP-64 and L-493) was directly suspended in 60 mL cultures of the laurate producing strain *Synechocystis* TE/Δslr1609. Culture was growed in the following condition: aerated with house air at a rate of 0.5 L/min, exposed to light at 100 μmol photon/m^2/s, and maintained at 30 ^oC. Samples of resin were removed from the culture at routine time intervals and their surfaces were imaged by SEM. The imaging results are compared in Figure 2.9 and 2.10 at different cell densities.

2.3 Results

2.3.1 Determination of adsorption isotherms.

Figure 2.2 shows the equilibrium isotherms determined for all 6 resins adsorbents studied, as well as the corresponding Langmuir model predictions.

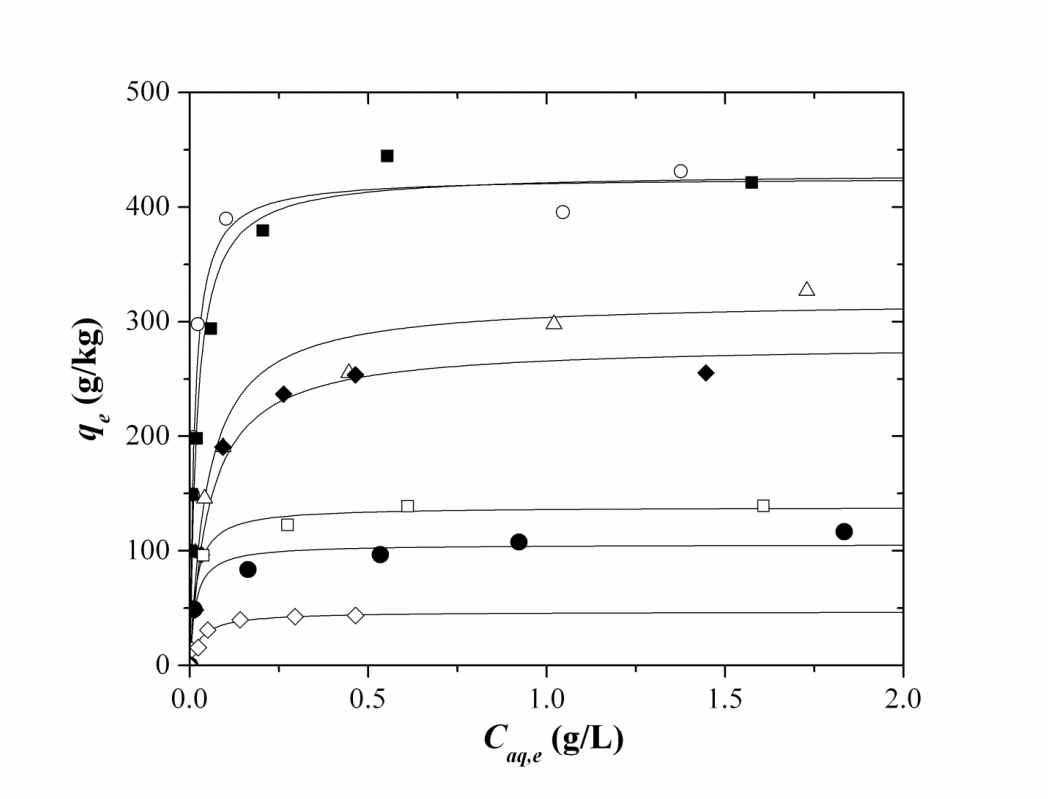

Figure 2.2 Experimental (shapes) and Langmuir-modeled (lines) equilibrium isotherms for laurate upon the screened adsorbents. Amberlite IRA-958 (closed diamond), Amberlite IRA-67 (open circle), Amberlite IRA-900 (open triangle), Amberlite IRA-402 (closed square), Dowex Optipore SD-2 (open square), Dowex Optipore L-493 (closed circle), and Carboxen 572 (open diamond).

By determining their equilibrium isotherms we can then determine the laurate adsorption capacity and affinity for each of the resin adsorbents studied. The Langmuir isotherm model (Equation 2.2) was found to provide the best overall fit for each of the isotherms, which suggests that under the conditions examined, adsorption of laurate on to the surface of resin likely occurs via single layer adsorption. Langmuir model parameters for each resin are summarized and compared in Table 2.2.

Table 2.2 Langmuir isotherm model parameters estimated for laurate adsorption upon each of the screened adsorbents.

Type	Adsorbent	q_{max} (g/kg)	K_d (g/L)	ΔG (kJ/mol)
Anion exchange	Amberlite IRA-958	280 ±17	0.055 ±0.024	-20.3 ±0.8
	Amberlite IRA-67	426 ±53	0.013 ±0.006	-23.9 ±1.7
Mixed-mode	Amberlite IRA-900	319 ±28	0.050 ±0.020	-20.5 ±1.5
	Amberlite IRA-402	430 ±35	0.020 ±0.011	-22.8 ±1.1
	Dowex Optipore SD-2	138 ±23	0.017 ±0.009	-23.2 ±1.1
Hydrophobic	Dowex Optipore L-493	106 ±15	0.016 ±0.007	-23.4 ±0.8
	Carboxen 572	47 ±8	0.030 ±0.015	-21.8 ±1.3

Again, q_{max} Table represents the maximum capacity for laurate, and so resin with a larger q_{max} can achieve a higher laurate recovery using the same adsorbent mass. As can be seen in Table 2.2, IRA-402 and IRA-67 (with anion exchange and mixed-mode functionalities, respectively) have the highest adsorption capacity. Comparing IRA-958 and IRA-67 (both of which only possess anion exchange functionality); their adsorption capacity is consistent with their anionic capacity: IRA-958's maximum capacity is 66% of that of IRA-67 while IRA-958 possesses an anionic capacity of 73% of IRA-67. This also demonstrates that adsorption by anion exchange resin only occurs via anion exchange mechanism. But although IRA-402 possesses an anionic capacity of only 3.8 meq/g (lower than even IRA-958), its mixed-mode functionality provides additional sites for laurate adsorption via hydrophobic interactions, allowing it to achieve a q_{max} of 430 g/kg. Although SD-2 has the smallest anionic capacity (only 0.8 meq/g), it still has a larger q_{max} than L-493 (pure hydrophobic adsorbent). Combined with the fact that L-493

has a larger surface area (the adsorption limiting feature of hydrophobic adsorbents) than SD-2, it might be concluded that anion exchange plays a more important role than hydrophobic interaction in laurate adsorption. In general, Table 1 demonstrates that, in terms of laurate capacity of polymer adsorbents, mixed mode ≥ anion exchange > hydrophobic. Moreover, low K_d values mean a higher affinity for laurate, that will allow efficient separation at lower concentrations. As predicted by Langmuir model, IRA-67 has the highest affinity for laurate. But it should be considered that higher affinity will bring problem to separation and recover process (i.e. require more energy input). Thus, K_d is a parameter in need of optimization upon considering all other relevant process variables. Also for all the resins studied they all show a much larger maximum loading capacity than Carboxen 572, even for L-493, which has the smallest maximum loading capacity among all resins, its q_{max} is still more than 2 times larger than that for Carboxen 572, indicating resins studied here have good affinity for laurate.

A more thorough understanding of adsorption process can be obtained by looking at energy change during adsorption. Gibb's free energy change can be used to quantify this by using the following equation (Liu 2006):

$$\Delta G^0 = RTln(K_d) \tag{2.8}$$

In which R is the universal gas constant and T is temperature. Gibb's free energy change for each kind of resin was estimated and compared in Table 2.2. Negative Gibb's free energy change means adsorption will happen spontaneously. Typically, ΔG^0 values of about -20 kJ/mol are found to be consistent with 'weak interactions' (Kuo, Wu et al. 2008; Ibezim-Ezeani and Anusiem 2011), including both electrostatic interactions involved with anion exchange as well as hydrophobic interactions (Klyosov, Mitkevich et al. 1986; Sugihara, Shigematsu et al. 2000). In this case, all ΔG^0 values were on the order of about -22 kJ/mol, which is consistent with adsorption by 'weak' interactions regardless of the

adsorption mechanism(s) exploited. Which will enable desorption process to be less energy demanding.

2.3.2 Investigating laurate adsorption kinetics.

Figure 2.3 compares the extent of laurate adsorption achieved as a function of time for each adsorbent studied.

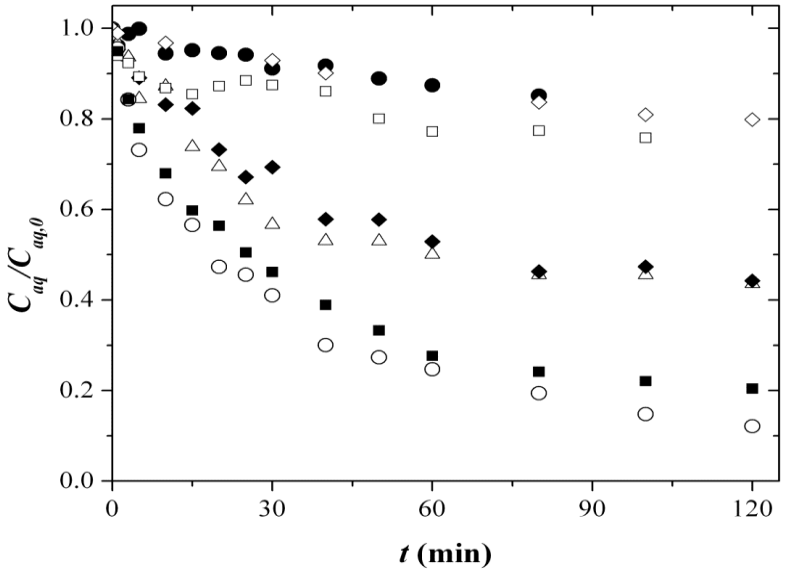

Figure 2.3 Kinetics of laurate adsorption for the adsorbents screened. Amberlite IRA-958 (closed diamond), Amberlite IRA-67 (open circle), Amberlite IRA-900 (open triangle), Amberlite IRA-402 (closed square), Dowex Optipore SD-2 (open square), Dowex Optipore L-493 (closed circle), and Carboxen 572 (open diamond)

As can be seen from Figure 2.3, equilibrium was approached by around 120 min, irrespective of adsorbent type (anion exchange, hydrophobic, or mixed-mode). Assuming the adsorbent particles to behave as perfect spheres with uniform properties, these kinetic data were then applied to each of pseudo first order, pseudo second order, and pore

diffusion kinetic models (Equations 2.4, 2.5 and 2.6, respectively). Mass transfer coefficients were estimated for the first two models while pore diffusivity was estimated for the third model. The results are compared in Table 2.3.:

Table 2.3 Comparing laurate adsorption kinetics for each of the screened adsorbents according to pseudo first order, pseudo second order, and pore diffusion models.

Type	**Resin**	k_1 **(min^{-1})**	k_2 **(*10^{-4} kg g^{-1} min^{-1})**	D_p **(*10^{-10} m^2/s)**
Anion exchange	Amberlite IRA-958	0.018	2.0	2.4
	Amberlite IRA-67	0.020	1.0	7.2
Mixed-mode	Amberlite IRA-900	0.024	0. 9	4.0
	Amberlite IRA-402	0.016	0. 8	5.1
	Dowex Optipore SD-2	0.009	0. 6	0.94
Hydrophobic	Dowex Optipore L-493	0.011	1.0	0.45
	Carboxen 572	0.002	0. 05	0.37

In this study, pore diffusion model was found to provide the best estimation (determined by minimization of SSE) and some of the comparisons (with IRA-67 represents anion exchange, IRA-402 represents mixed mode and L-493 represents hydrophobic resin) are shown in Figure 2.4. Also experimental data and pore diffusion model predictions are plotted together in Figure 2.5. As can be seen from Table 2.3, IRA-67 and IRA-402 possess the largest diffusion coefficients (7.2 and 5.1*10^{-10} m^2/s, respectively), indicating that these adsorbents support the fastest possible rates of laurate adsorption. In contrast to all other adsorbents, IRA-67 and IRA-402 are polymer gels (see Table 2.1), making them more amenable to swelling in aqueous solutions. Swelling of the adsorbent matrix enhances total porosity within the adsorbent particle which

facilitates intraparticle diffusion. Comparing D_p estimates in Table 2.3 with the adsorbent properties of Table 2.1, it can be seen that increased adsorbent swelling correlates with faster rates of adsorption, indicating that polymer gels can offer important kinetics advantages for the adsorption for long-chain FFAs, such as laurate.

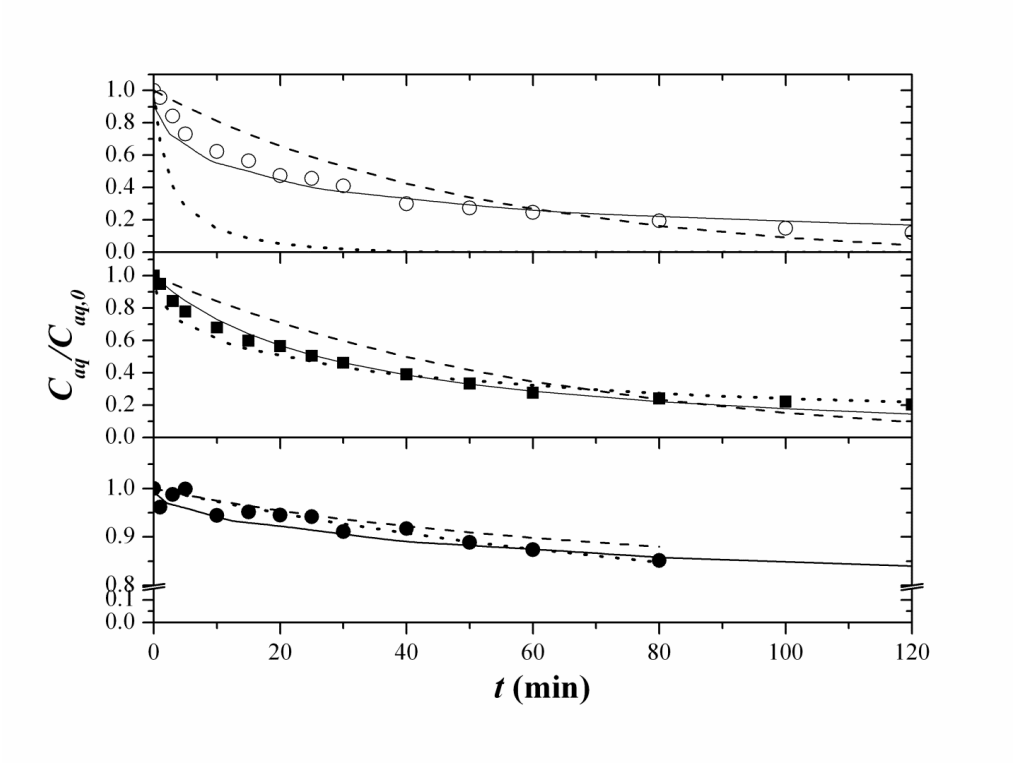

Figure 2.4 Comparing the fits of pseudo first order, pseudo second order, and pore diffusion models with experimental data for Amberlite IRA-67 (open circle), Amberlite IRA-402 (closed square), and Dowex Optipore L-493 (closed circle).

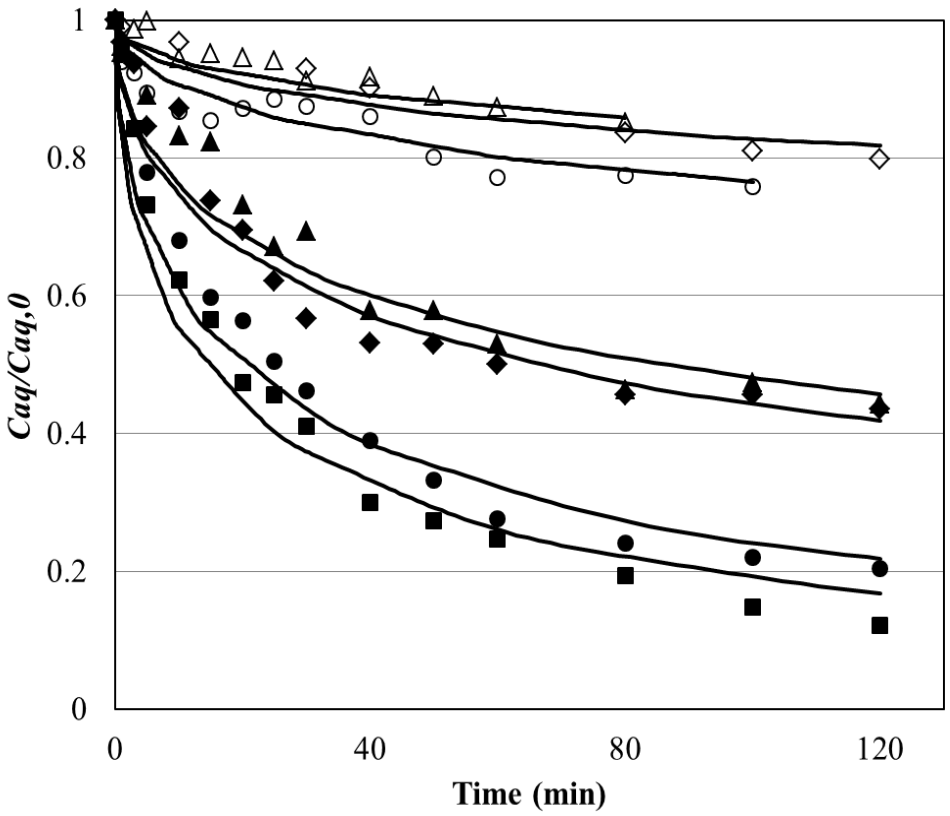

Figure 2.5 Kinetics of laurate adsorption for the adsorbents screened with solid lines for pore diffusion model predictions. Amberlite IRA-958 (closed triangle), Amberlite IRA-67 (closed square), Amberlite IRA-900 (closed diamond), Amberlite IRA-402 (closed circle), Dowex Optipore SD-2 (open circle), Dowex Optipore L-493 (open triangle), and Carboxen 572 (open diamond)

2.3.3 Investigating Breakthrough of Adsorption Beds

As can be seen from the Figure 2.6, t_b occurs at around 12.5 min at flow rates of 5 mL/min while breakthrough occurs almost immediately at flow rates of 10 mL/min. While this indicates that a lower flow rate results in a better performance in recovery laurate, separation was inefficient under all conditions examined. For example, at a 5 mL/min flow rate, by breakthrough the IRA-900 bed had adsorbed a total of 112 mg

sodium laurate. This corresponds to a loading capacity of only 28 g/kg, even though from prior equilibrium characterizations it is predicted that the loading capacity in equilibrium with an aqueous phase containing 2 g/L sodium laurate should be 319 g/kg, or more than 10-times larger. This means that the efficiency of the IRA-900 expanded bed adsorption column is quite low (8.8 %) even at a low flow rates, and certainly even worse as flow rate increases. Low efficiency in this case might result from slow adsorption kinetics. As discussed in above, nearly 2 h were required to reach equilibrium in batch adsorption studies, whereas the column residence time experienced at a flow rate of 5 mL/min was only 1.52 min. With this in mind, improved efficiency may be achieved by either using more resin to increase bed volume, by circulating the aqueous media through the column at lower rates, or by recycling the column effluent to allow further contact between unadsorbed solutes and the resin.

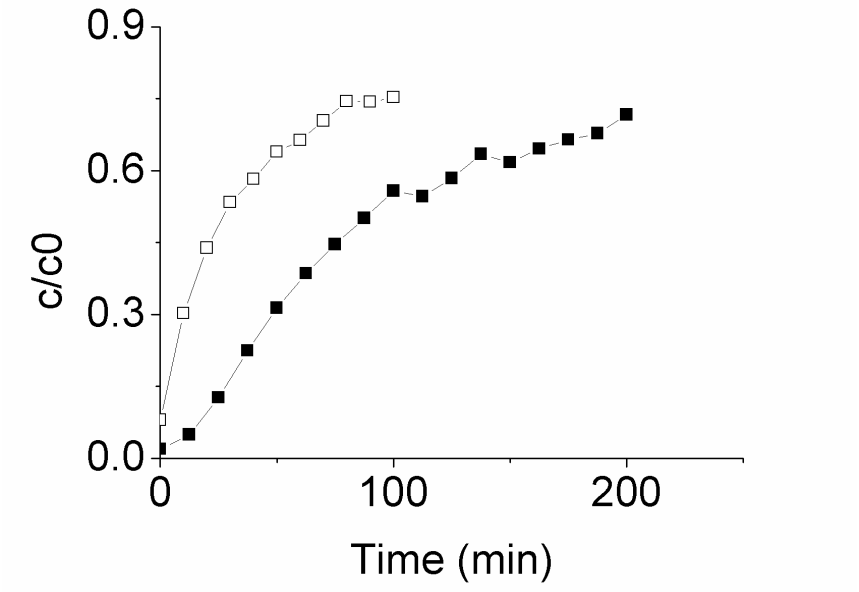

Figure 2.6 Relative sodium laurate concentration in effluent in breakthrough curve experiment with 5 mL/min (closed square) and 10 mL/min (open square) laurate solution

2.3.4 *In situ* recovery of lauric acid from cyanobacteria cultures by expanded bed adsorption

The effects of *in situ* laurate recovery by expanded bed adsorption on overall productivity and yield in photosynthetic cultures of *Synechocystis* TE/Δslr1609 was investigated. Cultures were either circulated through a fixed or expanded bed adsorption column of IRA-900, or in a traditional batch arrangement without any adsorbent as a control. It was realized early that fixed bed operation was unsuitable for this application since operation in this mode resulted in significant losses of cell viability upon circulation through the column (the culture was observed to turned yellow in color and cell density was reduced as compared to the control). Therefore this strategy was abandoned and the remainder of our study and we focused instead on the development and use of expanded bed adsorption.

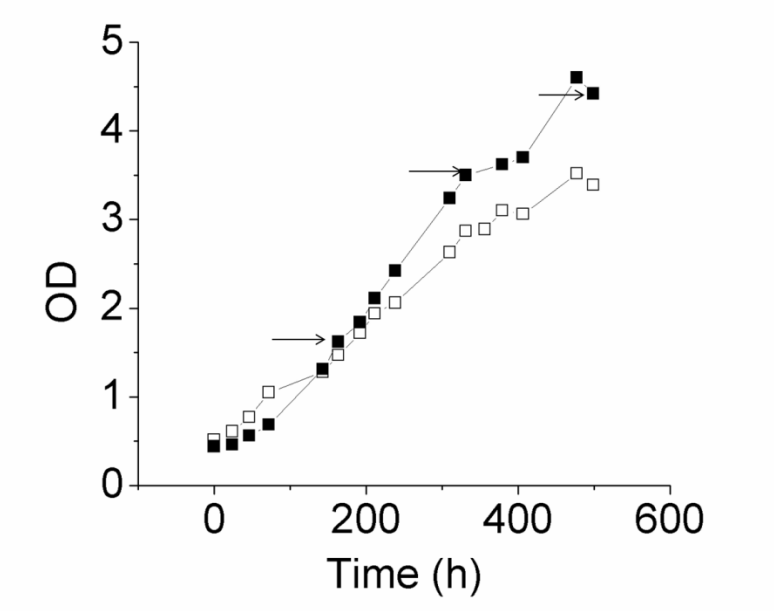

Figure 2.7 Comparison of OD for both control flask (open square) and flask coupled with resin column (closed square) with arrows indicating circulation begins

Figure 2.7 compares cell growth between the control and column circulated cultures, as measured by OD_{730}. It can be seen that although the control culture grew slightly faster initially, by about 163 h (which corresponds to when the circulation through the column first occurred); growth rates in the column circulated culture surpassed those of the control and continued in this manner for the duration of the experiment. By the end of the experiment, the column circulated culture had reached an OD_{730} of 4.42, or 30.4 % higher than that of the control (3.39). This change may have resulted due to the fact that as the culture medium was circulated through the adsorption column, the release of anions from the resins into the culture (recall that the column was pre-equilibrated with BG-11) could have afforded a superior growth environment. In fact, as seen in Figure 2.8, in column circulated cultures NO_3^- levels were found to be maintained nearly 3-fold higher than in the control, while Cl^- concentration also increased for column circulated culture while control remained almost the same during the whole process. For photoautotrophic microorganisms like *Synechocystis* PCC6803, the potential growth limiting factors include inorganic carbon, nitrogen, phosphorus, and photons from the irradiating light. Thus the potential for anion exchange resins to deliver nutrients to cultures 'on demand' is another potentially useful advantage of this *in situ* product recovery strategy.

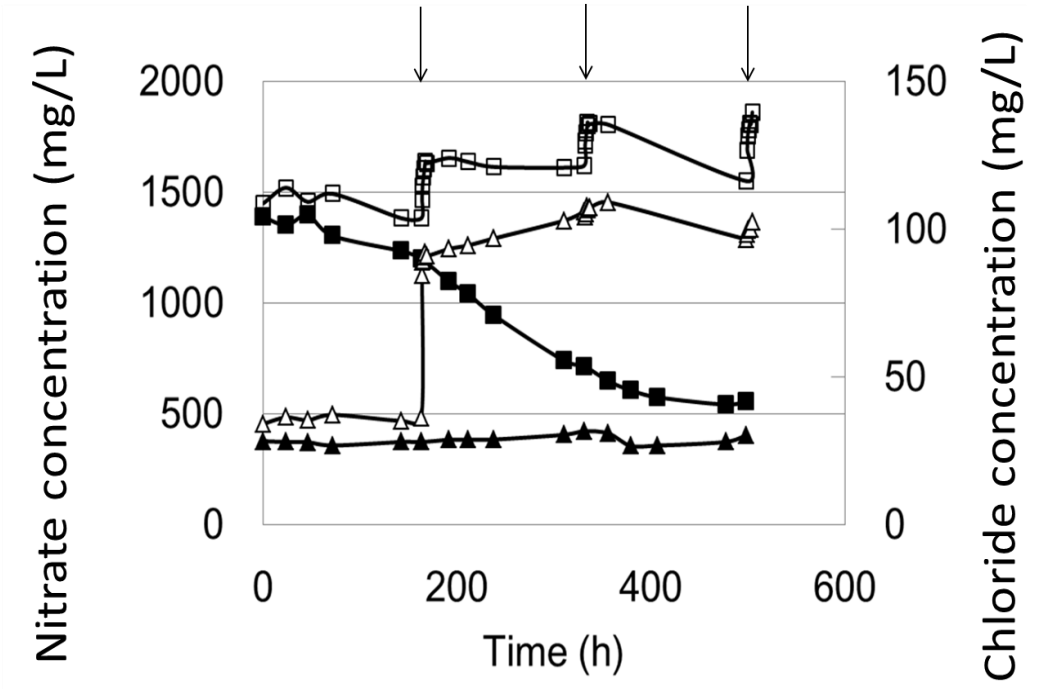

Figure 2.8 Comparison of key inorganic nutrient concentrations as a function of time, including Cl^- (closed triangle for control and open triangle for culture with column adsorption) and NO_3^- (closed square for control and open square for culture with column adsorption) with arrows indicating starting of circulation.

The adsorption effect of anion exchange resins on BG-11 media components was further investigated in a cell-free environment by adding different masses of IRA-900 (in its Cl^- form) to BG-11 and monitoring its effect on anionic nutrients at equilibrium. The results are compared in Figure 2.9. With pure BG-11 medium it can be seen that as resin concentration increased from 0 g/L to 10 g/L, aqueous Cl^- concentration increased dramatically from 16.3 mg/L to 419.4 mg/L. This was expected because, since the resin existed initially in its Cl^- form, as other anions were adsorbed Cl^- was released into the media. Meanwhile, each of NO_3^-, PO_4^{3-} and SO_4^{2-} were adsorbed onto the resin; while NO_3^-, the main nutrients for *Synechocystis*, decreased from 230.6 mg/L to 90.9 mg/L. This indicates that if one want to apply anion exchange resin to *in situ* laurate

recovery, to avoid depletion of nutrition resulting from adsorption by anion exchange resins, equilibration of resin with BG-11 medium is required.

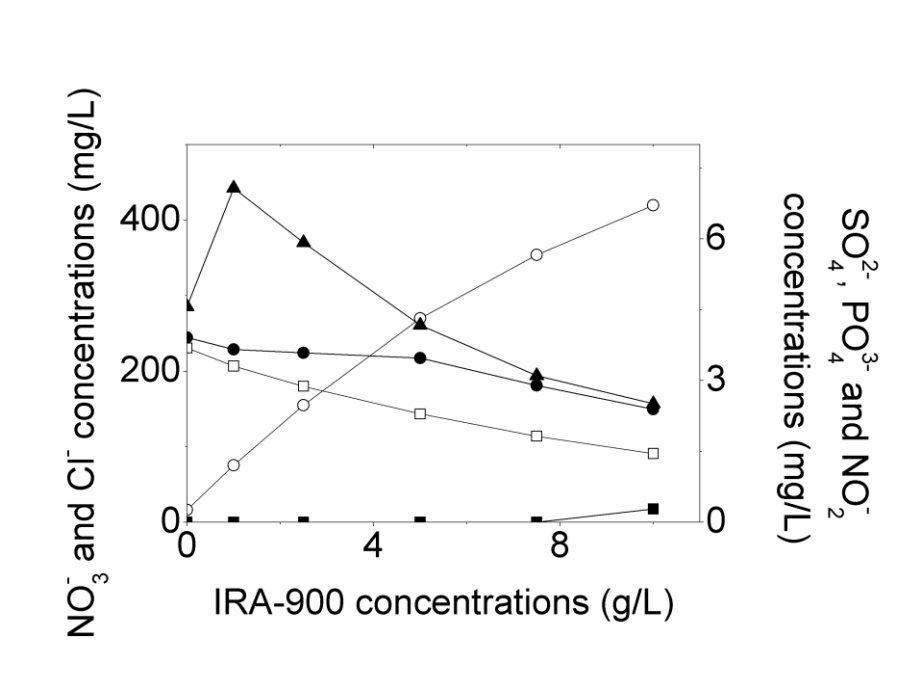

Figure 2.9 Anion concentrations in BG-11 with addition of different amount of IRA-900 with closed triangle for SO_4^{2-}, open circle for Cl^-, closed square for NO_2^-, open square for NO_3^- and closed circle for PO_4^{3-}.

Meanwhile, in addition to growth, differences in laurate production were also observed between the two cultures, as seen in Figure 2.10.:

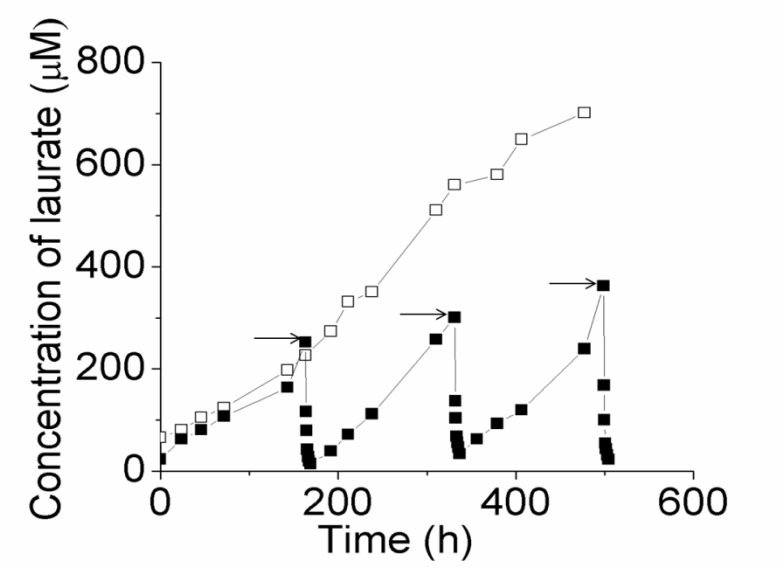

Figure 2.10 Comparison of laurate concentration for both control flask (open square) and flask coupled with resin column (closed square) with arrows indicating circulation begins

As can be seen from Figure 2.10, as a result of each of the three performed column circulation cycles, nearly all of the laurate that had previously accumulated in the aqueous phase was successfully removed in only ~5.5 h. Over the total 477 h experiment, the control culture produced about 700 μmol/L laurate whereas the column circulated produced about 744 μmol/L (a 6% increase), and this excess amount was produced almost all between second and third column extraction process, also suggesting that feedback inhibition at the pathway level does not have a big impact until lautate concentrations are larger than around 500 μmol/L.

2.3.5 Assessing the fouling potential of adsorbents by *Synechocystis*

The following section discusses the results from experiment that examined fouling of adsorbents by *Synechocystis* TE/Δslr 1609.

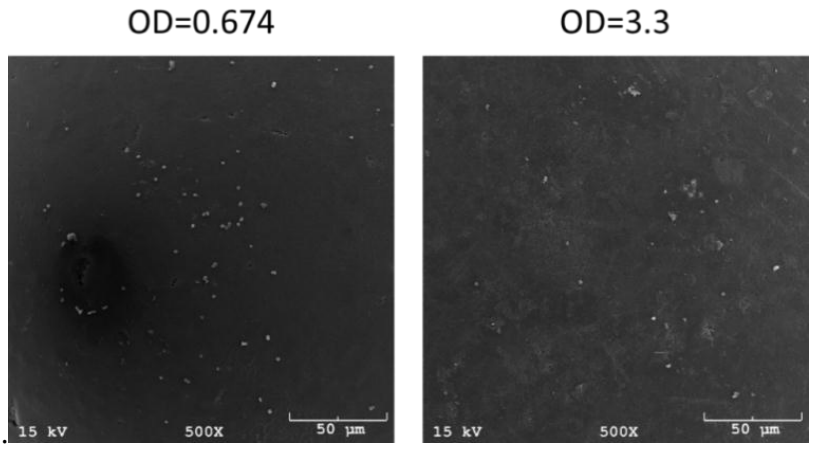

Figure 2.11 SEM images for resin IRA-900 at different OD_{730} of Synechocystis TE/Δslr1609

From figure 2.11 it can be seen that at both low and high cell density, only very few cells are observed to be surface associated, suggesting that fouling of IRA-900 was not a significant problem.

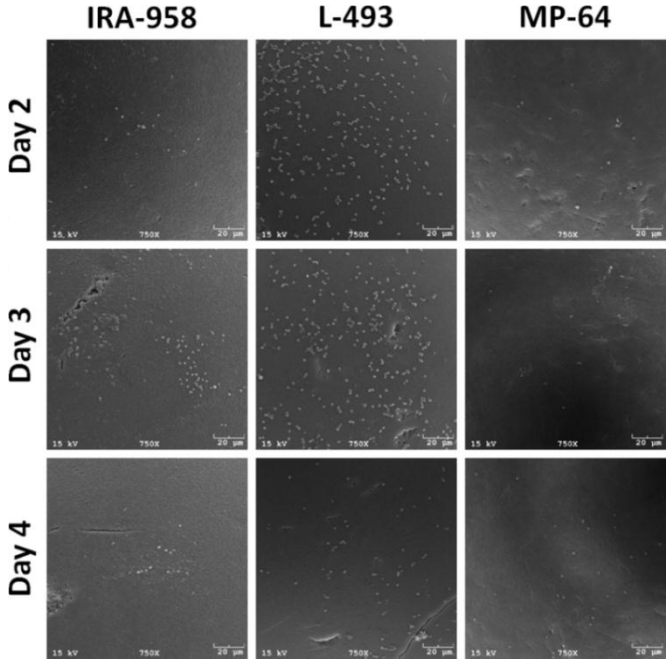

Figure 2.12 SEM images for resin IRA-958, L-493 and MP-64 at different time of Synechocystis TE/Δslr1609 growth

Bacterial attachment to a surface occurs through several mechanisms, including hydrophobic and electrostatic interactions (Roosjen, Mei et al. 2004; Park, Jang et al. 2007). Also researchers have found that control over hydrophobicity, surface roughness, electrostatic interactions, and surface compliance can dramatically reduce bacterial attachment (Mitik-Dineva, Wang et al. 2009). Therefore, additional experiments were also analogously conducted using three different adsorbent resins (IRA-958, L-493 and MP-64) to explore the potential impact of resin chemistry and/or functionalization on biofouling. Again it is seen from Figure 2.12 that for both IRA-958 (an anion exchange resin) and MP-64 (a mixed mode resin), only a few cells are on the surface of the resin, so fouling was not found to be problematic. Meanwhile, for L-493 (a hydrophobic resin), we observe many cells on the resin surface. Even still, however, there does not appear to be systematic fouling by biofilm formation. So it is expected that application of any of these resins to *in situ* laurate recovery should be acceptable in terms of minimal fouling.

For all the four resins studied, only L-493 showed substantial adsorption of *Synechocystis*. If we compare the functionality of these four resins (as shown in Table 2.1 with MP-64 has a tertiary and quaternary ammonium group), only L-493 is not functionalized with the other three all possessing cationic amine groups. It is known that polymers functionalized with cationic and quaternized moieties provide any effect means to render surfaces as antiseptic (Tiller, Liao et al. 2001; Haldar, An et al. 2006; Bouloussa, Rondelez et al. 2008). For example, in one early study, Tiller *et al*. covalently functionalized various common materials, including metals, polymers, and ceramics, with cationic poly(4-vinyl- N -alkylpyridinium bromide). The authors suggested that the introduction of poly cationic quaternary amine moieties provided the same growth inhibitory mechanism as antimicrobial peptides, that as cell penetration through interaction with cell wall components (Tiller, Liao et al. 2001). And so we postulate that

the cationic functional groups in IRA-900, IRA-958 and MP-64 may play the same role in our application and therefore prevent cells from adsorbing to the resin surface, and as L-493 lacks this functionality it is subjected to greater surface adsorption by cells.

2.4 Conclusions

Recovery of laurate from aqueous solutions can be effectively achieved by using polymer resin adsorbents, such as those investigated in this study. Amberlite IRA-402 (mixed-mode), IRA-67 (anion exchange), and IRA-958 (anion exchange) were found to possess the greatest capacities for laurate adsorption. Laurate adsorption capacity of adsorbents was strongly linked to their anionic capacity for both anion exchange and mixed-mode adsorbents. Laurate adsorption equilibria were well-described by the Langmuir isotherm model for all adsorbents, whereas adsorption kinetics were best represented by a pore diffusion model. Adsorption rates were fastest using polymer gel adsorbents as a result of increased particle swelling. Although preliminary investigations of expanded adsorption of laurate using Amberlite IRA-900 showed low efficiency, adsorption of laurate from cyanobacterial cultures by this same approach were effective for product removal. Furthermore, the inclusion of ion exchange resins in cultures appeared to improve cell growth and product formation, possibly as a result of their ability to deliver anionic nutrients when appropriately equilibrated in BG-11 medium. Fouling of adsorbent surfaces by cells was not found to be prevalent in cultures up to 4 days in age.

Chapter 3

CHARACATERIZATION OF NOVEL MAGNETIC MESOPOROUS CARBON POWDERS FOR BIOFUEL ALCOHOL ADSORPTION

3.1 Materials and Methods

3.1.1 Chemicals.

n-butanol (HPLC grade, >99.7%) was purchased from Sigma-Aldrich (St. Louis, MO). Ethanol (200 proof) was purchased from VWR international (Radnor, Pennsylvania).

3.1.2 Analytical methods.

All alcohol concentrations were analyzed by high pressure liquid chromatography (HPLC; 1100 series, Agilent, Santa Clara, CA) with ZORBAX Eclipse XDB-C18 column (Agilent, Santa Clara, CA) and operated at 50 ^{o}C. Filtered and degassed deionized water are used as mobile phase at a flow rate of 1 mL/min. Alcohols are detected by a refractive index detector (RID).

3.1.3 Synthesis and characterization of magnetic particles.

Magnetic mesoporous carbon powder adsorbents used in this study were synthesized in collaboration with the laboratory Dr. Bryan D. Vogt (formerly of at Arizona State University) and his student Mingzhi Dai. The powder CS-68-800 was synthesized according to the protocol of previous work (Levario, Dai et al. 2012). Different concentrations of $Co(acac)_3$ was added to CS-68-800 precursor solution (0.208 g TEOS, 0.1 g resol, and 0.1 g Pluronic F127) to synthesize three different CS-Co-X-800

powders. X stands for the content of $Co(acac)_3$ in the precursor. The precursor solution was heated to 45 ℃ for 2 h, and then spread to a few watch-glasses. They were allowed to evaporate ethanol in air at room temperature overnight and then thermally cross-linked at 120 ℃ for 24 h. Scraping powders from watch-glasses and performing carbonization in tubular furnace under nitrogen atmosphere with a flow rate of 140 cm^3/min at 800 ℃ for 2 h with heating rates of 1 ℃ /min below 600 ℃, and 5 ℃/min above 600 ℃ will result in the final product. X-ray diffraction (XRD) was performed in a θ/2θ geometry using Cu Kα source (Panalytical X'Pert PRO) with 2θ varied from 0.5 to 3.0° for small angle XRD (mesostructure) and from 10 to 80 °for wide angle XRD (crystal structure). Specific surface areas were calculated using the Brunauer–Emmett–Teller (BET) method in a relative pressure range of P/P0 = 0.05–0.25. The pore size distribution (PSD) and pore volume were estimated from the adsorption branch of the isotherm using the Barrett–Joyner–Halenda (BJH) model. Transmission electron microscopy (TEM) was performed on powder materials using JEOL 2010F microscope operating at 200 keV.

3.1.4 Equilibrium adsorption of alcohol biofuels.

To determine the adsorption isotherm behavior novel adsorbent powders, about 20–40 mg each powders was added to a 1-1.5 mL solution of either ethanol or *n*-butanol in a 1.8mL HPLC vial. Solutions were prepared in deionized water at initial concentrations ranging from 2.5-140 g/L (or 54-3043 mmol/L) ethanol or from 1-60 g/L (or 14-811 mmol/L) *n*-butanol. Sample vials were placed in a 37 ^oC incubator where they shook at 200 rpm for 24 hours. A temperature of 37 ^oC was selected due to its relevance with respect to many important biofuel fermentations. After equilibrium was reached, samples of the aqueous supernatant were removed (using pipette filter tips to exclude the magnetic powders in suspension) and analyzed by HPLC for alcohol concentration.

Specific loading of alcohols adsorbed to powders at equilibrium (q_e) was again determined by using Equation 2.1. Equilibrium adsorption data was then fit to either Langmuir or Freundlich isotherm models by the methods described in Section 2.1.3.1, and best fit model parameters were determined by minimizing sum of square errors (SSE).

3.1.5 Investigation the kinetics of alcohol adsorption.

In this experiment, 20 mg CS-Co-4-800 was added to 1.5 mL solutions of both 40 g/L ethanol and 30 g/L *n*-butanol in water. Due to the small volume used, 6 batch adsorption experiments were conducted in parallel, each being sampled at a different point; namely after 30 s, 1min, 2 min, 5 min, 15 min and 30 min. All samples were mixed on a Vortex Genie 2.0 (Scientific Industries; Bohemia, New York) at 1000 rpm until sampling for HPLC analysis. Equilibration was determined by comparing loading capacity to model predictions from the equilibrium adsorption experiments.

3.1.6 Assessing the biocompatibility of magnetic mesoporous carbon adsorbents.

The biocompatibility of CS-Co-10-800 was tested with respect to three different biofuel-producing microorganisms: *E. coli* KO11, *S. cerevisiae* BY4741 and *C. acetobutylicum* ATCC 824. Cells were grown both in the presence and absence (control) of different masses of CS-Co-10-800 powder. For both *E. coli* KO11 and *S. cerevisiae* BY4741, growth was tested under both aerobic and anaerobic conditions, whereas *C. acetobutylicum* ATCC 824 could only be tested anaerobically. For *E. coli* KO11, Luria Broth (LB) with glucose was used as growth medium. The formulation of LB is as follows: tryptone 10 g/L, yeast extract 5 g/L and NaCl 10 g/L. To prepare the medium, 5 mL of LB and 5 mL 20% (wt) glucose were added to a culture tube. Chloramphenicol (34 mg/L) was also added as an antibiotic to protect against contamination (note that *E.*

coli KO11 carries a Cm^R marker). Yeast Extract Peptone Dextrose (YPD) media was used for *S. cerevisiae* growth. The formulation of YPD is as follows: yeast extract 10 g/L, peptone 20 g/L, and glucose 10 g/L. *C. acetobutylicum* ATCC 824 was grown in Clostridium Growth Media (CGM) with glucose at an initial concentration of 80 g/L. Components in CGM media has the following concentration: $(NH_4)_2SO_4$: 2 g/L, K_2HPO_4: 0.75 g/L, KH_2PO_4: 0.75 g/L, $MgSO_4 \cdot 7H_2O$: 0.712 g/L, $FeSO_4 \cdot 7H_2O$: 0.01 g/L, $MnSO_4 \cdot H_2O$: 0.01 g/L, NaCl: 1 g/L, yeast extract: 5 g/L, asparagine: 2 g/L and cysteine HCl: 0.5 g/L. Resazurin was used as an oxygen indicator with a concentration of 5 mg/L. Both *E. coli* KO11 and *S. Cerevisiae* BY4741 were first inoculated from plates stored in 4 ^oC into the liquid media to prepare a seed. After 24 hours the seed was then used to inoculate fresh media both with and without CS-Co-10-800 powder. *C. acetobutylicum* ATCC 824 was first inoculated from frozen stock stored at -80 ^oC into anaerobic tube containing reinforced clostridium media (RCM) to prepare a seed culture. After 24 hours the seed was then used to inoculate fresh tubes of CGM media both with and without CS-Co-10-800 powder. Recipe for RCM media is as following: yeast extract: 3.0 g/L, 'Lab-Lemco' powder: 10.0 g/L, peptone: 10.0 g/L, glucose: 5.0 g/L, soluble starch: 1.0 g/L, sodium chloride: 5.0 g/L, sodium acetate: 3.0 g/L, cysteine hydrochloride: 0.5 g/L and agar: 0.5 g/L. Growth was used in all cases as a measure of biocompatibility and was assessed by measuring optical density as a function of time.

3.2 Results

3.2.1 Characterization of magnetic particles

The physical properties of the magnetic mesoporous carbon powders used in this study are summarized in Table 3.1. To facilitate comparison; the properties of other 3 previously studied biofuel adsorbents are also included in Table 3.1.

Table 3.1 Comparing the physical properties of magnetic mesoporous carbon powders used in this study, as well other previously studied biofuel adsorbents.

	Surface area (m^2/g)	Pore Diameter (nm)	Pore Volume (cm^3/g)	Co ratio (wt%)
CS-Co-1-800	1809	4.0	1.68	0.85
CS-Co-4-800	1393	4.1	1.28	2.09
CS-Co-10-800	1125	4.2	0.99	4.78
FDU-16-800	671	5.8	0.14	0
CS-68-800	1287	8.2	1.39	0
L-493	>1100	4.6	1.16	0

As can be seen from Table 3.1, CS-Co-X-800 powders showed Co content from 0.89 to 4.78 % when the $Co(acac)_3$ concentration was increased from 1 % to 10 %. Changing in Co level in the carbon framework also affected the surface area, which varied from 1809 to 1125 cm^2/g. CS-Co-1-800 showed the highest surface area and pore volume, which is likely due to the fact that Co acts to mechanically strengthen the framework of the powder during carbonization to partially suppress volumetric contraction.

As can be seen from transmission electron microscopy (TEM) in Figure 3.1, when $Co(acac)_3$ level was below 10 %, all CS-Co-X-800 materials maintained the same ordered mesoporous structure as CS-68-800. The loss of long range ordering of CS-Co-10-800 sample was likely due to the aggregation of nanoparticles in the carbon framework. While there were no obvious nanoparticles observed in CS-Co-1-800 (since the Co level was so low), nanoparticles were seen to be distributed uniformly in CS-Co-

4-800. However, the size of the magnetic particles was found to increase greatly in CS-Co-10-800, leading to a disordered structure.

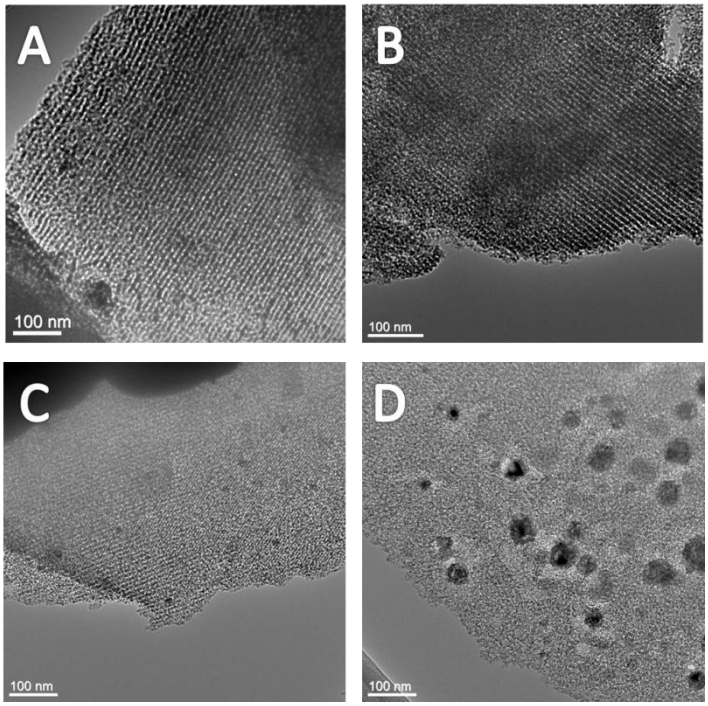

Figure 3.1 TEM images for (A) CS-68-800, (B) CS-Co-1-800, (C) CS-Co-4-800 and (D) CS-Co-10-800.

3.2.2 Characterization of adsorption isotherms.

Based on the equilibrium adsorption data, Freundlich model was found to provide the best fit for all the adsorption isotherms (by minimizing standard deviation). Experimental data and Freundlich model predictions are plotted in Figure 3.2 and Freundlich model parameters are summarized in Table 3.2.:

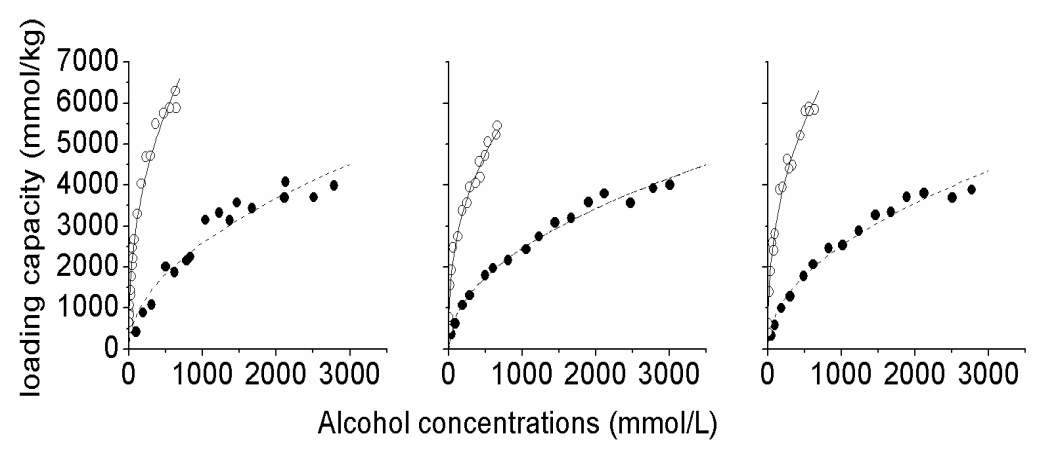

Figure 3.2 Experimental (symbols) and Freundlich model predictions (lines with solid for n-butanol and dashed for ethanol) for ethanol (closed circles) and n-butanol (open circles) adsorption equilibria with (A) CS-Co-1-800, (B) CS-Co-4-800, (C) CS-Co-10-800

Table 3.2 Freundlich model parameters estimated for both ethanol and n-butanol with all magentic mesoporous carbon powders investigated.

	Ethanol		*n*-butanol	
Adsorbent	k_F (mmol/kg)	*n*	k_F (mmol/kg)	*n*
CS-Co-1-800	80.7 ±71	1.99 ±0.47	470 ±105	2.48 ±0.24
CS-Co-4-800	86.9 ±31	2.07 ±0.20	461.3 ±90	2.66 ±0.23
CS-Co-10-800	83.5 ±39	2.03 ±0.26	483.6 ±114	2.55 ±0.26

By comparing k_F and *n* it can be seen that both k_F and *n* for *n*-butanol are larger than those for ethanol for all three kinds of powders, seems those parameters are positively correlated with alcohol carbon chain length. The larger the hydrophobicity of alcohol or the higher the adsorption capacity of magnetic particles, the larger the Freundlich parameters are.

As can be seen from Table 3.1, from CS-Co-1-800 to CS-Co-4-800 and then to CS-Co-10-800, surface area as well as pore volume decreases. Surface area decreases from 1809 to 1125 m^2/g and pore volume decreases from 1.68 to 0.99 cm^3/g. But it can be seen from adsorption isotherm plot as well as Freundlich parameters that all three kinds of magnetic particles possess almost the same capacity for both ethanol and *n*-butanol in the concentration range studied. This is in contrast to the general accepted idea that the larger the surface area the higher the loading capacity. The reason for this requires further study but one hypothesis would be the limited of usage of total surface area, perhaps as a result of intraparticle transport limitations.

It can be seen from Figure 3.2 that all three magnetic powders displayed a much higher affinity for *n*-butanol than they did for ethanol. The difference can be directly and quantitatively described by determining the ratio q_{eq}/C_{eq} (loading capacity of adsorbent divided by aqueous phase concentration at adsorption equilibrium), which is akin to a partitioning or distribution coefficient. For example, for CS-Co-1-800, at an equilibrium aqueous concentration of ~500 mmol/L (23g/L for ethanol and 37g/L for *n*-butanol), q_{eq}/C_{eq} for ethanol is only about 3.66 while for *n*-butanol it is more than three times larger at 11.56. This in turn demonstrates that the adsorption occurs by hydrophobic interactions (i.e., van der Waals forces); because *n*-butanol is much more hydrophobic than ethanol its adsorption benefits from a larger driving force. Gibb's free energy change during adsorption was also estimated by using the following relationship (Huang, Zhou et al. 2007):

$$\Delta G = -RTn \tag{3.1}$$

In which R is universal gas constant, T is temperature and n is Freundlich exponent. The results are compared in Table 3.3.

Table 3.3 Predicted Gibb's free energy change for adsorption of ethanol and n-butanol with each magentic mesoporous carbon powder studied

Carbon powder	ΔG (kJ/mol) Ethanol	ΔG (kJ/mol) *n*-butanol
CS-Co-1-800	-5.1	-6.4
CS-Co-4-800	-5.3	-6.9
CS-Co-10-800	-5.2	-6.6

As can be seen from Table 3.3, for all the magnetic particles, Gibb's free energy change for *n*-butanol is slightly larger than that for ethanol, as is consistent with a higher adsorption driving force. In addition, all the values of Gibb's free energy change are smaller than 20kJ/mol which, as discussed in section 2.3.1, is consistent with the fact that the interactions between magnetic particles and alcohols occur via 'weak interactions' that include hydrophobic interactions.

The adsorption performance of all three magnetic mesoporous carbon powders for *n*-butanol was also compared to that of one commercially available polymer resin adsorbent, L-493, and two previously developed non-magnetic mesoporous carbons, all of which were the subject of prior biofuel separation studies. Relevant properties of these previously studied adsorbents are also summarized in Table 3.1. Figure 3.3 compares the equilibrium performance of these materials with the adsorbents of interest to this study, as indicated from Freundlich isotherm model predictions.

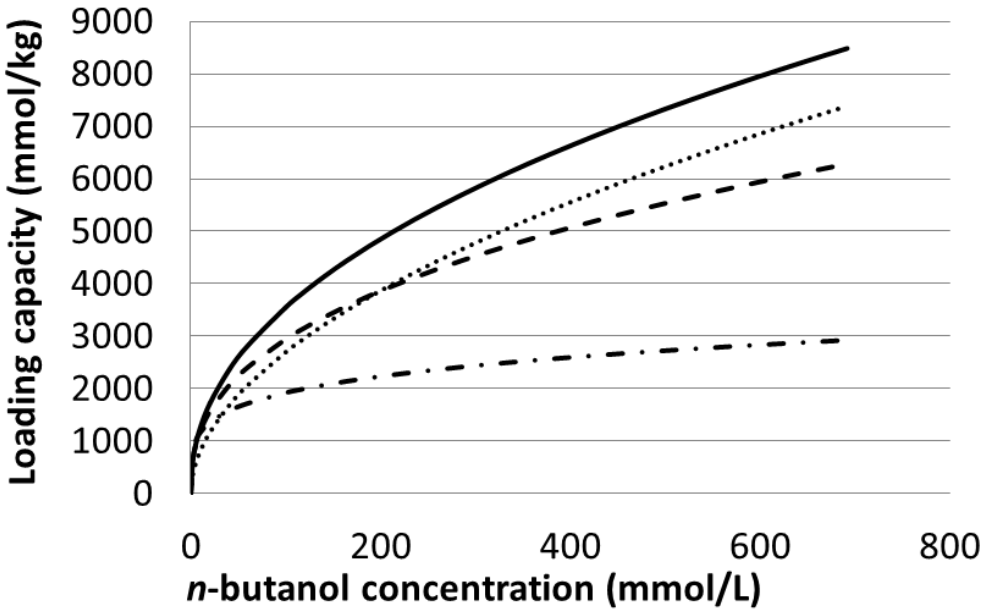

Figure 3.3 Comparison of n-butanol adsorption isotherms of L-493 (line), CS-68-800 (round dot), CS-Co-10-800 (dash) and FDU-16-800 (dash dot)

It can be seen that for *n*-butanol, the three magnetic particles in this study perform better than FDU-16-800 but not as well as either CS-68-800 or L-493. L-493 performs best of four kinds of adsorbents in terms of maximum loading capacity. The poorer performance of FDU-16-800 relative to other adsorbents may have resulted due to its relatively low surface area (only about 671 m^2/g where as other three all have a surface area larger than 1000 m^2/g). Although CS-Co-10-800 performed worse than CS-68-800 at higher *n*-butanol concentrations (greater than 200mmol/L, or 14.8 g/L), it was noticed that under more dilute concentration (which are more representative of the conditions observed in the ABE fermentation), CS-Co-10-800 has a higher equilibrium loading capacity than CS-68-800. For example, at an equilibrium concentration of 40 mmol/L, CS-68-800 has a loading capacity of 1673 mmol/kg while CS-Co-10-800 has a loading capacity of 2057 mmol/kg, about 23% higher. Thus, the magnetic mesoporous

particles may still have potential advantages over CS-68-800 for in *in situ n*-butanol recovery applications.

From the above discussion, it can be seen that magnetic particles have an excellent capacity for *n*-butanol adsorption, and certainly much higher than for ethanol. Based on the adsorption mechanism, it can be predicted that magnetic particles should also be effective at adsorbing other hydrophobic second generation biofuels such as *n*-butanol, iso-butanol, *n*-pentanol, for example.

3.2.3 Investigating the kinetics of ethanol and *n*-butanol adsorption.

Based on kinetic experiments results, aqueous alcohol concentrations as a function of time are plotted in Figure 3.4.:

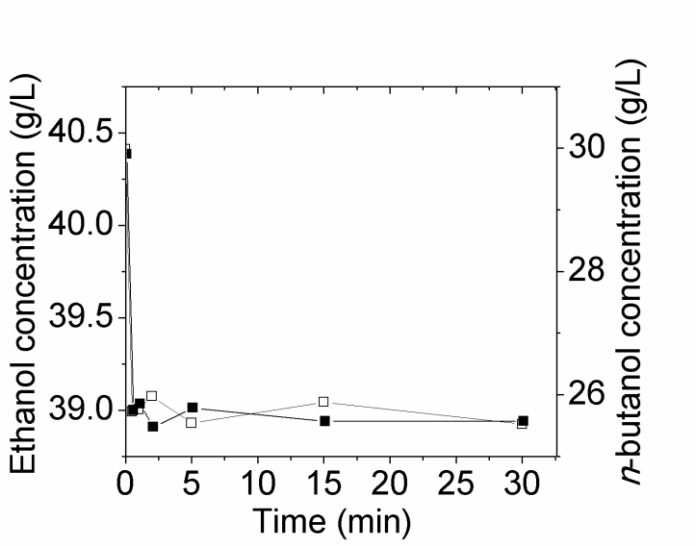

Figure 3.4 Alcohol concentration change during kinetic adsorption for both ethanol (open squares) and n-butanol (closed squares) with CS-Co-4-800

As can be seen from Figure 3.4, in only 30 seconds residual aqueous concentrations of both *n*-butanol and ethanol had reached steady-state. Furthermore, by

comparing the average loading capacity at each steady state (average of all data between 5 and 30 min), as these values were found to agree well with the respective Freundlich isotherm models (Table 3.4), it can be concluded that the system had reached equilibrium within just 30s. When compared to a commercially available adsorbent L-493 for *n*-butanol adsorption studied by Nielsen *et al.* (2009), although L-493 has a higher capacity for *n*-butanol as discussed in adsorption isotherm section, it will take almost 116 min for them to reach equilibrium, at least 232 times longer than CS-Co-4-800 (Nielsen and Prather 2009). L-493 is a macroporous resin made of poly(styrene-co-divinylbenzene), it doesn't have uniform pore structure as CS-Co-4-800, FDU-16-800 and CS-68-800. The random pore structure produces a more tortuous path for intraparticle diffusion of *n*-butanol before it can access the surface 'sites' for adsorption within the adsorbent matrix. Thus, adsorption kinetics for L-493 is much slower than the other 3 adsorbents. Meanwhile, when also compared to the mesoporous carbons (FDU-16-800 and CS-68-800) examined by Levario *et al.* (2012), which reached equilibrium in about 1 to 6 min (Levario, Dai et al. 2012), magnetic particles studied here display faster adsorption rates than FDU-16-800 and similar rates to CS-68-800.

Table 3.4 Comparison of actual loading capacity and Freundlich model predictions for the data presented in Figure 3.4.

Alcohol	Actual loading(g/kg)	Freundlich model predictions (g/kg)
EtOH	105	104
n-BuOH	315	308

Another important consideration when applying any adsorbent for *in situ* product recovery is that the adsorption rate it displays should be greater than the maximum production rate of the inhibitory product of interest. Taking this into consideration, CS-

Co-4-800, FDU-16-800 and CS-68-800 might provide additional advantage although they have a smaller loading capacity than L-493. For example, in the case studied in this kinetic experiment, CS-Co-4-800 has an adsorption rate of 8400 g ethanol/(L•h•g CS-Co-4) and 25200 g *n*-butanol/(L•h•g CS-Co-4), much higher than the reported ethanol production rate (2.88 g/(L•h) of *Z. mobilis* ZM4 (Pinilla, Torres et al. 2011)) and *n*-butanol production rate (0.32g/(L•h) of *C. beijerinckii* BA101) (Ezeji, Qureshi et al. 2004)). This indicates adsorption kinetic does not limit the application of magnetic particles to *in situ* product recovery, provided ample adsorbent is used.

3.2.4 Assessing the biocompatibility of magnetic mesoporous carbon powders.

The growth of each of *S. cerevisiae* BY4741 and *C. acetobutylicum* ATCC 824, they showed almost complete inhibition by CS-Co-10-800, as summarized in Table 3.5. Meanwhile, the growth of *E. coli* KO11 was found to be severely inhibited under analogous conditions.

Table 3.5 Effect of CS-CO-10-800 addition on the growth of different model microbes.

Strain	Aerobic	Powder (g)	Anaerobic	Powder (g)
S. cerevisiae BY 4741	DNG*	0.215	DNG	0.2
E. coli KO 11	Inhibited	0.19	Inhibited	0.1
C. acetobutylicum ATCC 824	N/A	N/A	DNG	0.215

* means did not grow

The most likely reason for the inhibitory action of these adsorbents is the presence of Co in the adsorbent. Although cobalt is an essential nutrient for bacteria and required as trace elements at nanomolar concentrations, at micro- or millimolar

concentrations, Co^{2+} is toxic. Yang *et al.* (2008) previously studied the effects of cobalt-induced inhibition of *E. coli* DH5α using two model compounds: bis(salicylideniminato-3-propyl)methylaminocobalt(II) (denoted as Co(II)) and Co(III) sepulchrate trichloride (denoted as $Co(sep)^{3+}$). By adding different concentrations of these compounds to growing cultures it was determined that the half-inhibitory concentrations (IC_{50}) of Co(II) and $Co(sep)^{3+}$ to *E. coli* DH5α were 15 and 42.1 μg/mL with lethal dose of 40 and 332.5 μg/mL, respectively. The mechanism of toxicity was also studied by using scanning electron microscopy and demonstrated that the two cobalt compounds had the same toxic mechanism on *E. coli* DH5α, which was attributed to the damage of cell wall of the bacteria caused by both Co(II) and $Co(sep)^{3+}$ (Yang, Xu et al. 2008). In an earlier study by Ram *et al.* (1999), the effects of cobalt on bacterial activity during anaerobic oxidation of organic matter, particularly on sulfate reducing bacteria (SRB) and methane producing bacteria (MPB), it was found that the addition of 5 mmol/L Co^{2+} inhibited both SRB and MPB cells' activity (Ram, Singh et al. 2000).

One method to solve the toxicity problem caused by these adsorbents could be to cover them with biocompatible coatings. For example, *S. cerevisiae* can be used to convert L-phenylalanine to 2-phenylethanol. But researchers have shown that concentrations of 2-phenylethanol larger than 2.9 g/L have a negative impact on the oxidative capacity of the yeast. To avoid this problem, *in situ* product recovery using organic solvents can be used, but organic solvents are frequently toxic. To solve this problem, Serp *et al.* (2002) entrapped a toxic organic solvent (dibutylsebacate) in a polymeric matrix of polyethylene to form a highly absorbent and chemically and mechanically stable composite resin. It was found that the composite resin successfully prevented phase toxicity while still selectively extracting 2-phenylethanol from the

culture medium. This approach increased the volumetric productivity of 2-phenylethanol by a factor of 2 (Wyss, Boucher et al. 2006).

Another method to address adsorbent toxicity could be achieved by using immobilization of cells. Kanda *et al.* (1998) used this approach to protect baker's yeast from the toxicity caused by the organic solvent isooctane. It was found that double entrapment (further entrapment of calcium-alginate-gel-entrapped cells with a urethane prepolymer), made it possible for the yeast to remain viable in isooctane. Furthermore, doubly entrapped living yeast cells could carry out the stereoselective reduction in isooctane repeatedly for a long period (more than 1200 h) with occasional cultivation (Kanda, Miyata et al. 1998). Thus, immobilization of cell enabled it to survive in toxic organic environment over long-term, and could be employed to aid in address the toxicity caused by our magnetic powders.

3.3 Conclusions

Adsorption isotherm experiments showed a very high loading capacity of all three kinds of magnetic particles, with a higher affinity for *n*-butanol than ethanol. The three magnetic particles showed almost the same adsorption capacity for both ethanol and *n*-butanol and the Freundlich model was found suitable for modeling each adsorption isotherm. Preliminary results on adsorption kinetics showed that magnetic particles achieve very quick adsorption for both ethanol and *n*-butanol. Unfortunately, however, the magnetic powders all showed strong inhibition against three model biofuel producing microbes. Before the magnetic particles can be used to *in situ* product recovery, the issue of toxicity problem must first be solved, perhaps by using either biocompatible coatings on the adsorbent particles or immobilization of the cells.

Chapter 4

SUGGESTED FUTURE WORK

Based on the results from this thesis, the following future works are recommended:

1) For breakthrough curve experiment with polymer resins, test performance of other resins studied in this work for both fixed bed and expanded, find ways to increase bed efficiency; it's also better to study a laurate concentration that is similar to that in culture.
2) For adsorption kinetic experiment with magnetic particles, perform some more batch experiment with time points between 0 s and 30 s, model adsorption kinetics. Finish kinetic experiment with other two kinds of powder and compare adsorption kinetics of the three kinds of powders.
3) Test fouling of magnetic particles by adding powder to solution with media components such as pure glucose solution and yeast extract solution or alcohol solution with glucose and yeast extract to see if there is competition.
4) Try to solve magnetic particle toxicity by either using biocompatible coatings or immobilizing cells. If this works, perform further experiment by adding powder to culture and see if adsorbent can efficiently recover alcohol biofuels and achieve a higher titer than control in batch fermentations.
5) Try to make use of magnetism of magnetic particles and facilitate separation of adsorbent from aqueous solution.

REFERENCES

Ackers, P. (1982). "Standard Methods for the Examination of Water and Wastewater." Water Res. **16**: 1495-1497.

Adnađević, B., Z. Mojović, et al. (2007). "The kinetics of ethanol adsorption from the aqueous phase onto zeolite NaZSM-5." Adsorption **14**(1): 123-131.

Anvari, M., H. Pahlavanzadeh, et al. (2009). "In situ recovery of 2,3-butanediol from fermentation by liquid-liquid extraction." J Ind Microbiol Biotechnol **36**(2): 313-317.

Baez, A., K. M. Cho, et al. (2011). "High-flux isobutanol production using engineered Escherichia coli: a bioreactor study with in situ product removal." Appl Microbiol Biotechnol **90**(5): 1681-1690.

Bandini, S. and C. Gostoli (1992). "Ethanol removal from fermentation broth by gas membrane extraction." Journal of Membrane Science **70**: 119-127.

Bouloussa, O., F. Rondelez, et al. (2008). "A new, simple approach to confer permanent antimicrobial properties to hydroxylated surfaces by surface functionalization." Chem Commun (Camb)(8): 951-953.

Bravo, B., J. Sanchez, et al. (2008). "Partitioning of fatty acids in oil/water systems analyzed by HPLC." Journal of Surfactants and Detergents **11**(1): 13-19.

Cook, T. E., W. A. Cllley, et al. (1982). "Zeolite A hydrolysis and degradation." Environmental Science Technology **16**: 344-350.

Dhamole, P. B., Z. Wang, et al. (2012). "Extractive fermentation with non-ionic surfactants to enhance butanol production." Biomass and Bioenergy **40**: 112-119.

El-Zanati, E., E. Abdel-Hakim, et al. (2006). "Modeling and simulation of butanol separation from aqueous solutions using pervaporation." Journal of Membrane Science **280**(1-2): 278-283.

Ezeji, T. C., N. Qureshi, et al. (2003). "Production of acetone, butanol and ethanol by Clostridium beijerinckii BA101 and in situ recovery by gas stripping." World Journal of Microbiology & Biotechnology **19**: 595-603.

Ezeji, T. C., N. Qureshi, et al. (2004). "Butanol fermentation research: upstream and downstream manipulations." Chem Rec **4**(5): 305-314.

Garc á, V., J. P äkkil ä, et al. (2011). "Challenges in biobutanol production: How to improve the efficiency?" Renewable and Sustainable Energy Reviews **15**(2): 964-980.

Groot, W. J. and K. C. A. M. Luyben (1986). "In Situ Product Recovery By Adsorption Of Butanol/Isopropanol Batch Fermentation." Applied Microbiology and Biotechnology **25**: 29-31.

Haldar, J., D. An, et al. (2006). "Polymeric coatings that inactivate both influenza virus and pathogenic bacteria." Proc Natl Acad Sci U S A **103**(47): 17667-17671.

Huang, H. H., Y. Zhou, et al. (2007). "Adsorption behavior, thermodynamics, and mechanism of phenol on polymeric adsorbents with amide group in cyclohexane." Journal of Colloid and Interface Science **316**(1): 10-18.

Ibezim-Ezeani, M. U. and A. C. I. Anusiem (2011). "Thermodynamics of the adsorption of palmitate and laurate soaps onto some metal ore surfaces in aqueous media." African Journal of Pure and Applied Chemistry **5**(9): 272-277.

Jones, R. A., J. A. Gandier, et al. (2011). "Enhanced ethanol production through selective adsorption in bacterial fermentation." Biotechnology and Bioprocess Engineering **16**(3): 531-541.

Kaewkannetra, P., N. Chutinate, et al. (2011). "Separation of ethanol from ethanol–water mixture and fermented sweet sorghum juice using pervaporation membrane reactor." Desalination **271**(1-3): 88-91.

Kanda, T., N. Miyata, et al. (1998). "Doubly entrapped baker's yeast survives during the long-term stereoselective reduction of ethyl 3-oxobutanoate in an organic solvent." Appl Microbiol Biotechnol **49**: 377-381.

Klyosov, A. A., O. V. Mitkevich, et al. (1986). "Role of the Activity and Adsorption of Cellulases in the Efficiency of the Enzymatic-Hydrolysis of Amorphous and Crystalline Cellulose." Biochemistry **25**(3): 540-542.

Kuo, C. Y., C. H. Wu, et al. (2008). "Adsorption of direct dyes from aqueous solutions by carbon nanotubes: Determination of equilibrium, kinetics and thermodynamics parameters." Journal of Colloid and Interface Science **327**(2): 308-315.

Lalman, J. A. and D. M. Bagley (2004). "Extracting long-chain fatty acids from a fermentation medium." Journal of the American Oil Chemists Society **81**(2): 105-110.

Laluce, C., J. O. Tognolli, et al. (2009). "Optimization of temperature, sugar concentration, and inoculum size to maximize ethanol production without significant decrease in yeast cell viability." Appl Microbiol Biotechnol **83**(4): 627-637.

Levario, T. J., M. Dai, et al. (2012). "Rapid adsorption of alcohol biofuels by high surface area mesoporous carbons." Microporous and Mesoporous Materials **148**(1): 107-114.

Lin, Y. L. and H. P. Blaschek (1983). "Butanol Production by a Butanol-Tolerant Strain of Clostridium acetobutylicum in Extruded Corn Broth." APPLIED AND ENVIRONMENTAL MICROBIOLOGY, **45**: 966-973.

Liu, H. S. and H. W. Hsu (1990). "Analysis of gas stripping during ethanol fermentation—I. In a continuous stirred tank reactor." Chemical Engineering Science **45**: 1289-1299.

Liu, X., D. Brune, et al. (2010). "Production and secretion of fatty acids in genetically engineered cyanobacteria." Proc Natl Acad Sci U S A.

Liu, Y. (2006). "Some consideration on the Langmuir isotherm equation." Colloids and Surfaces a-Physicochemical and Engineering Aspects **274**(1-3): 34-36.

Maddox, I. S. (1982). "Use of silicalite for the adsorption of n-butanol from fermentation liquors." Biotechnology Letters **4**: 759-760.

Magnuson, K., S. Jackowski, et al. (1993). "Regulation of fatty acid biosynthesis in Escherichia coli." Microbiological Reviews **57**: 522-542.

Martik, J., M. Rosenberg, et al. (1995). "Toxicity of organic solvents used in situ microbial fermentation." Biotechnol Tech **9**(4): 247-252.

Matsumoto, T., S. Ishikawa, et al. (2004). "Construction of ethanol-tolerant yeast strains with combinatorial library-selected peptides." Journal of Molecular Catalysis B: Enzymatic **28**(4-6): 253-257.

Mitik-Dineva, N., J. Wang, et al. (2009). "Escherichia coli, Pseudomonas aeruginosa, and Staphylococcus aureus attachment patterns on glass surfaces with nanoscale roughness." Curr Microbiol **58**(3): 268-273.

Nielsen, D. R., G. S. Amarasiriwardena, et al. (2010). "Predicting the adsorption of second generation biofuels by polymeric resins with applications for in situ product recovery (ISPR)." Bioresour Technol **101**(8): 2762-2769.

Nielsen, D. R. and K. J. Prather (2009). "In situ product recovery of n-butanol using polymeric resins." Biotechnol Bioeng **102**(3): 811-821.

Oudshoorn, A., L. A. M. van der Wielen, et al. (2009). "Adsorption equilibria of bio-based butanol solutions using zeolite." Biochemical Engineering Journal **48**(1): 99-103.

Park, S. N., H. J. Jang, et al. (2007). "Preparation and characterization of biodegradable anti-adhesive membrane for peritoneal wound healing." J Mater Sci Mater Med **18**(3): 475-482.

Pinilla, L., R. Torres, et al. (2011). "Bioethanol production in batch mode by a native strain of Zymomonas mobilis." World J Microbiol Biotechnol **27**: 2521-2528.

Qureshi, N., M. M. Meagher, et al. (2001). "Acetone butanol ethanol (ABE) recovery by pervaporation using silicalite–silicone composite membrane from fed-batch reactor of Clostridium acetobutylicum." Journal of Membrane Science **187**: 93-102.

Qureshi, N., B. C. Saha, et al. (2008). "Butanol production from wheat straw by simultaneous saccharification and fermentation using Clostridium beijerinckii: Part I—Batch fermentation." Biomass and Bioenergy **32**(2): 168-175.

Ram, M. S., L. Singh, et al. (2000). "Effect of ion, nickel and cobalt on bacterial activity." Water, Air, and Soil Pollution **117**: 305-312.

Roffler, S. R., H. W. Blanch, et al. (1987). "In situ extractive fermentation of acetone and butanol." Biotechnology and Bioengineering **31**: 135-143.

Roosjen, A., H. C. v. d. Mei, et al. (2004). "Microbial Adhesion to Poly(ethylene oxide) Brushes Influence of Polymer Chain Length and Temperature." Langmuir **20**: 10949-10955.

Saravanan, V., D. A. Waijers, et al. (2010). "Recovery of 1-butanol from aqueous solutions using zeolite ZSM-5 with a high Si/Al ratio; suitability of a column process for industrial applications." Biochemical Engineering Journal **49**(1): 33-39.

Sharma, P. and W.-J. Chung (2011). "Synthesis of MEL type zeolite with different kinds of morphology for the recovery of 1-butanol from aqueous solution." Desalination **275**(1-3): 172-180.

Shi, Z., C. Zhang, et al. (2005). "Performance evaluation of acetone-butanol continuous flash extractive fermentation process." Bioprocess Biosyst Eng **27**(3): 175-183.

Silvestre-Albero, A., J. Silvestre-Albero, et al. (2009). "Ethanol removal using activated carbon: Effect of porous structure and surface chemistry." Microporous and Mesoporous Materials **120**(1-2): 62-68.

Sugihara, G., D. S. Shigematsu, et al. (2000). "Thermodynamic study on the Langmuir adsorption of various bile salts including taurine and glycine conjugates onto graphite in water." Langmuir **16**(4): 1825-1833.

Thomas, K. C., S. H. Hynes, et al. (1996). "Practical and theoretical considerations in the production of high concentrations of alcohol by fermentation." Process Biochemistry **31**: 321-331.

Tiller, J. C., C. J. Liao, et al. (2001). "Designing surfaces that kill bacteria on contact." Proc Natl Acad Sci U S A **98**(11): 5981-5985.

Veeraraghavan, S. and L. T. Fan (1989). "Modeling adsorption in liquid—solid fluidized beds." Chemical Engineering Science **44**: 2333-2344.

Walker, G. (1998). Yeast growth. Yeast: Physiology and Biotechnology. G. Walker. New York, Wiley**:** 101-202.

Wyss, A., J. Boucher, et al. (2006). "Micro-encapsulated organic phase for enhanced bioremediation of hydrophobic organic pollutants." Enzyme and Microbial Technology **40**(1): 25-31.

Y. Isono and M. Nakajima (1999). "Application of hydrophobic membrane for alcohol separation from alcohol aqueous biphase mixture." Separation and Purification Technology **17**: 77-82.

Yang, L. N., F. Xu, et al. (2008). "A microcalorimetric study of the toxicity of two cobalt compounds on Escherichia coli DH5α growth." Journal of Thermal Analysis and Calorimetry **93**.

Yomano, L. P., S. W. York, et al. (2008). "Re-engineering Escherichia coli for ethanol production." Biotechnol Lett **30**(12): 2097-2103.